AD

INTRINSIC AND THERMAL STRESS MODELING FOR THIN-FILM MULTILAYERS TECHNICAL REPORT

A. M. Ledger and R. C. Bastien
The Perkin-Elmer Corporation
Norwalk, Connecticut 06856

Contract No. DAAA-25-76-C-0410

June 1977

~~Contract No. DAA25-76-C-0410~~

DEFENSE ADVANCED RESEARCH PROJECTS AGENCY
1400 WILSON BOULEVARD
ARLINGTON, VIRGINIA 22209

Distribution of this document is unlimited

AD

INTRINSIC AND THERMAL STRESS MODELING FOR THIN-FILM MULTILAYERS

TECHNICAL REPORT

A. M. Ledger and R. C. Bastien
The Perkin-Elmer Corporation
Norwalk, Connecticut 06856

Contract No. DAAA-25-76-C-0410

June 1977

~~Contract No. DAA25-76-C-0410~~

DEFENSE ADVANCED RESEARCH PROJECTS AGENCY
1400 WILSON BOULEVARD
ARLINGTON, VIRGINIA 22209

The findings in this report are not to be construed as an official Department of the Army position unless so designated by other authorized documents.

TABLE OF CONTENTS

TABLE OF CONTENTS (Continued)

LIST OF ILLUSTRATIONS

LIST OF ILLUSTRATIONS (Continued)

SECTION 1

INTRODUCTION

Multilayer dielectric coatings fabricated by thermal evaporation exist in a stressed condition due to intrinsic stress buildup during deposition, combined with temperature-induced stress changes established during post-deposition cooling. The intrinsic stress levels found in thin films depend primarily upon film thickness but are also influenced for some materials by the evaporation rate and substrate temperature during deposition. After the film is formed in a vacuum at a given temperature, a reversible stress change can occur due to differential contraction of film and substrate during cooling, and in some cases an irreversible stress change occurs when the film is vented to air. These stress levels greatly influence the durability of thin film structures when utilized under extreme thermal conditions such as in high energy laser systems.

Although stress levels in growing film structures have been measured and widely reported during recent decades, little progress has been made in establishing a quantitative link between induced stress and coating reliability for multilayer dielectric coatings. The measurement of stress in thin film structures is only one important aspect of the durability problem; the other is the adhesion between film and substrate and between individual films in a multilayer stack. For instance, certain films can be deposited in a highly stressed condition and show good durability, a good example being chromium which shows an intrinsic stress ($\sim$ 10,000 kg/cm^2) two or three times greater than most materials. Evaporated deposits of chromium adhere so strongly that the glass substrate undergoes surface rupture as the film thickness approaches 1-μm thickness.

The present program was initiated to develop stress and adhesion models for multilayer dielectric coatings in an attempt to predict the reliability and durability of thin film coatings. In particular, stress models of anti-reflection coatings for high expansion window materials such as potassium chloride and calcium fluoride were studied, since such materials produce large thermally induced stress changes in the antireflection coating materials when subjected to high-power laser beams.

This report describes a stress measurement system, stress models for thin films, and stress and material property measurements of thorium tetrafluoride, zinc selenide and thallium iodide films for use as materials for antireflection coatings on potassium chloride at 10.6 μm.

A new stress interferometer that measures both the magnitude and sign of the intrinsic stress in a coating during deposition was developed during the program and is described in Section 2. A system of four such stress interferometers equipped with an automatic data recording system was utilized in conjunction with a 36-inch box coating facility to characterize the stress profiles of several antireflection coating materials.

Stress models for multilayer coatings were also reviewed during the program and a computer code was completed to enable thermal stress modeling of multilayer coatings to be carried out. This theoretical phase is described in Section 3.

The intrinsic stress behavior of two infrared coating materials, thorium tetrafluoride and zinc selenide, was investigated in detail together with the stress properties of thallium iodide and cerium fluoride (Section 4).

Section 5 discusses a new method of measurement of the expansion coefficient and Young's modulus for thin film materials using the stress interferometer system.

SECTION 2

STRESS MEASUREMENTS IN THIN FILMS

2.1 STRESS MEASUREMENT TECHNIQUES

Thin films used for antireflection coatings in the 10-μm region are deposited in thicknesses of 1 to 2 μm depending upon refractive index, and stress data has not previously been measured for such "thick" film structures. Previous measurement methods and experimental results for the stress properties of metal and dielectric films have been comprehensively reviewed by Hoffman (Refs. 1,2) and Kinosita (Ref. 3).

The intrinsic stresses developed in metal films have been measured by many authors to develop theories of film nucleation and growth; however, stresses developed in dielectric films have not been investigated as thoroughly. The two most comprehensive investigations of stress buildup in dielectric films were carried out by Campbell (Ref. 4) and Ennos (Ref. 5). The stress behavior of various fluorides, bromides and iodides (LiF, NaF, NaCl, NaBr, KBr, KI) have been measured by Campbell using a capacitance bridge method, whereas Ennos used a laser interferometer to measure intrinsic stress in a large variety of coating materials (ZnS, MgF_2, $ThOF_2$, PbF_2, cryolite, chiolite, CaF_2, CaF_3, SiO, $PbCl_2$, TlCl, TlI, Ge, Te, CdTe) as a function of their deposition conditions. Many different measurement techniques can be utilized for the measurement of intrinsic stress, most of which depend upon detecting the minute deflections of a thin glass beam or disk upon which the film is being deposited. Optical interference methods provide a very sensitive method of measuring such small deflections although capacitative and electro-mechanical methods can also provide comparable sensitivities. The measurement of stress using electron diffraction as carried out by Halliday (Ref. 6) and X-ray diffraction techniques reported by Kinabara (Ref. 7) can also be used, but such techniques are not so easily implemented as are the bending beam and disk methods.

Although stress data exist for many of the materials utilized for antireflection coatings for KCl windows, the measurements only provide the intrinsic stress up to film thicknesses of several thousand angstroms. The use of new materials, higher deposition temperatures and deposition rates together with improved vacuum systems necessitated remeasurement of thin film stresses for such thick films during the present program.

---

1. R.W. Hoffman, Physics of Thin Films, Vol. 3, p. 211 (1966).
2. R.W. Hoffman, Thin Solid Films, Vol. 34, p. 185 (1976).
3. K. Kinosita, Thin Solid Films, Vol. 17, p. 17 (1972).
4. R.S. Carpenter and D.S. Campbell, J. Matl. Sci., Vol. 2, p. 173 (1967).
5. A.E. Ennos, Applied Optics, Vol. 5, No. 1, p. 51, (1966).
6. J.S. Halliday, T.B. Rymer, and K.H.R. Wright, Proc. Roy. Soc., London A225, 548 (1954).
7. A. Kinabara, H. Harabi, J. Appl. Phys., (Japan), Vol. 4, p. 243 (1965).

Laser interferometry was chosen as the most useful technique, and a system of four interferometers together with an automatic data recording system was designed and fabricated for use with a 36-inch metal box coating unit. This system enables stress measurements to be made rapidly and reproducibly for a variety of substrate configurations and deposition conditions and is described in detail in this section.

2.2 STRESS MEASUREMENTS - SYSTEM REQUIREMENTS

The principal problem occurring in any of the stress-measurement techniques mentioned previously is a thermal one. The amount of bending detected in a beam or disk is due to both the buildup of intrinsic stress in the depositing film and any nonuniform temperature existing radially or across the thickness of the disk. Calculations of the deflections expected for typical stress levels in a thin film (1000 - 3000 kg/cm^2) show that they are comparable to thermally induced distortions caused by front to back or radial gradients in the thin substrate. Since deposition usually occurs at a fixed substrate temperature, such gradients can be initially minimized; however, thermal energy from the source, heaters, and shutters can provide disturbing thermal fluxes and extreme care must be exercised to understand and compensate for these factors if reproducible measurements are to be made.

The use of large disks or beams of extremely small cross section (50 to 100 μm) increases the stress measurement sensitivity since the disk deflection is proportional to the square of the aspect ratio (D/d). Unfortunately, thin disks are also increasingly susceptible to temperature effects and the release of built-in stresses caused by polishing. Since stress data are primarily required for thick films ($\sim \lambda/4$ at 10.0 μm) for the present study, one can utilize thick substrates in the 0.25- to 1.0-mm range. Accurate stress measurements can be made using thick substrates if deflections are recorded at a rapid rate on paper tape during deposition. The use of thick substrates not only minimizes vibration problems and thermal effects but also allows many other different materials, such as ZnSe, ZnS, Ge, KCl, to be used to form the deformable substrate. It is not usually possible to polish such materials to thicknesses of 50 to 100 μm without suffering a very low polishing yield and the use of such thin disks or beams becomes impractical for experimental purposes.

At the outset of the program, a list of required measurement capabilities was established to enable stress measurements to be made for both single and multilayer films deposited under the kinds of conditions found in practice in fabricating 10.6-μm antireflection coatings. These capabilities included the use of:

- Multiple stress interferometers to enable stress measurements to be made for different film materials on both flexible and rigid substrates during same evaporation cycle by the use of remote shutters
- Accurate deposition rate control by the use of a crystal film thickness monitor that controls the input power to the source (electron gun)
- Variable vapor-incidence angles possible at each interferometer

- Rigid substrates (KCl) at equivalent deposition positions and incidence angles
- Both electron-gun sources and resistance sources
- Accurate optical film-thickness monitoring using a white-light source and spectral filter or monochromator
- Enclosed heater assembly to maintain the interferometers, optical monitor, and rigid substrates at elevated temperatures up to 250°C
- A semiautomatic data acquisition system to enable substrate deflection data and optical film thickness to be recorded on paper tape for subsequent computer data reduction

Four individual interferometers were designed and fabricated and mounted on a 36-inch stainless-steel box coater to enable the stress behavior of different combinations of two or more thin-film materials to be investigated during a single pumpdown. By the use of remote shutters and four interferometers, stress data can be obtained for materials A and B alone as well as for materials B on A and A on B on four different flexible and rigid substrates. The details of the interferometer design, coating chamber configuration, and data processing equipment are briefly described in the following paragraphs.

2.3 STRESS INTERFEROMETER - CAT'S EYE DESIGN

A previous laser interferometer system used at Perkin-Elmer by Ennos (Ref. 5) consisted of a Michelson interferometer that detected changes in deflection of a thin fused silica beam supported at both ends by ceramic knife edges. The deflecting substrate forms one mirror of the interferometer and the output fringe pattern consists of line fringes that move past a fixed detector as the substrate deflects.

In practice, this type of interferometer configuration was found to be sensitive to vibration, and distortion of the interferometer occurred at high temperatures. Recently, a high temperature Michelson interferometer designed for UHV applications has been described by Roll and Hoffman (Ref. 8). Thermal distortions are minimized in this design by obtaining an interferogram of the full aperture of the bending disk and by deducing the deflection from successive photographs of the fringe pattern. Tilts and axial displacements of the substrate can be removed by computation but the method requires substantial data reduction time for each successive fringe pattern taken during deposition.

Thermal distortions and angular tilts between the two interferometer mirrors can be virtually eliminated if the distance between the two reflecting surfaces is made very small and if the interferometer is arranged in the form of a cat's eye as shown in Figure 1.

The interferometer consists simply of a glass element whose front surface is polished to focus the incident laser beam onto two reflecting surfaces

---

8. K. Roll and H. Hoffman, Rev. Sci. Inst., Vol. 47, No. 9 (1976).

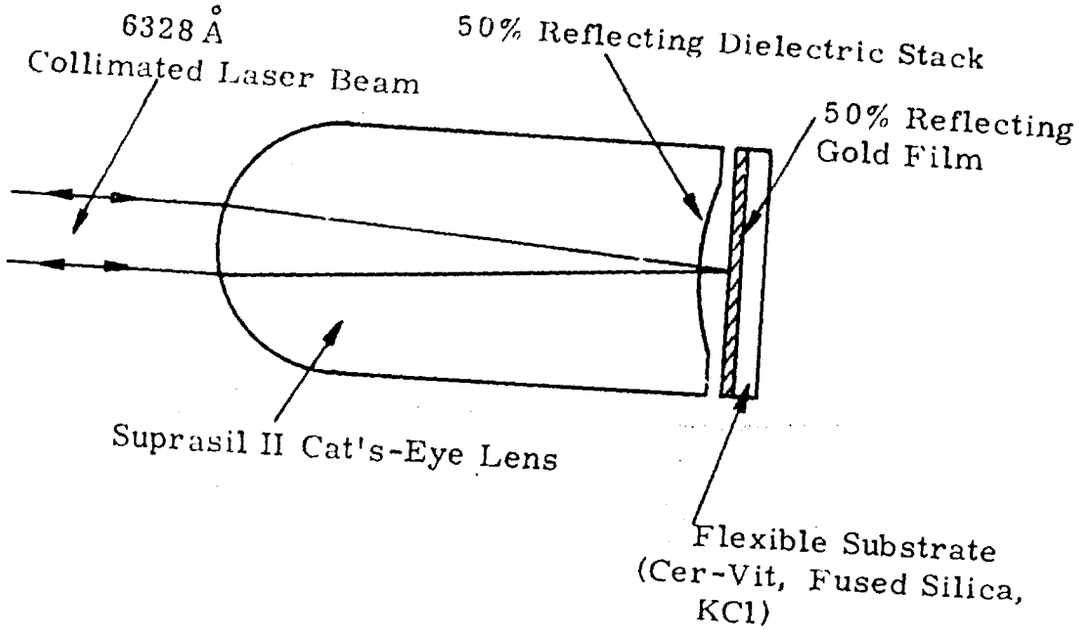

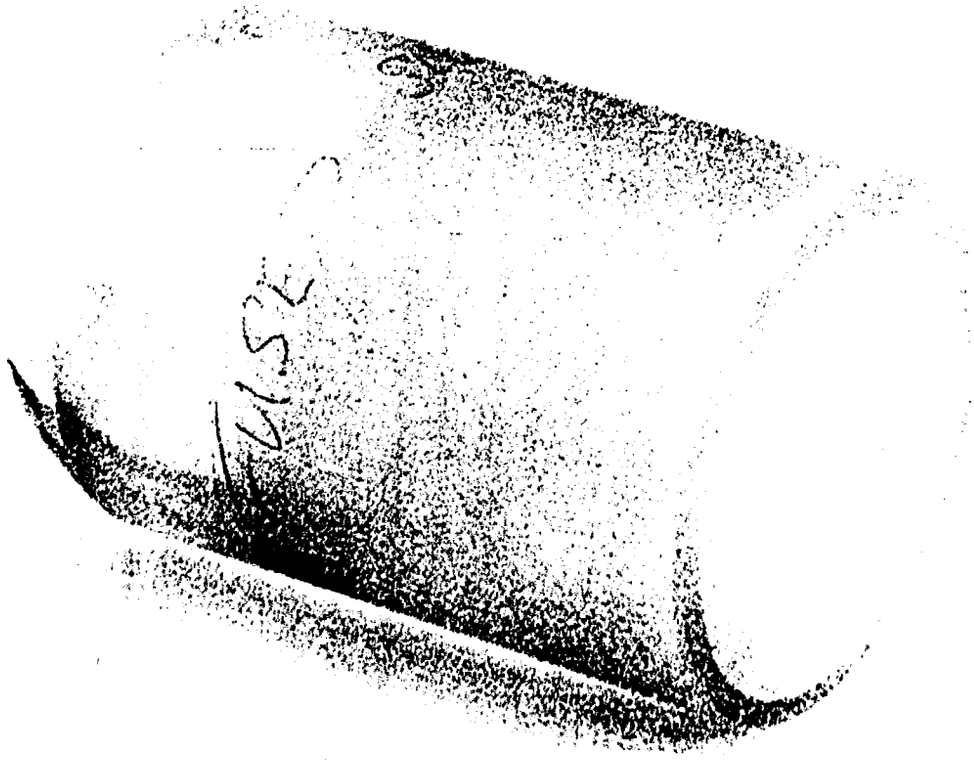

Figure 1. Cat's-Eye Interferometer

formed by the base of the cat's eye lens and the substrate upon which the film is being deposited. The base of the lens is coated with a hard dielectric reflector to reflect ~50% of the incident beam at 6328 Å and the deformable substrate is coated on its top surface with a partially reflecting metal coating. In most experiments a gold coating was used for this purpose since, when cold-deposited, gold has a low stress and has such poor adhesion to the substrate that it can be easily wiped from the surface. In addition, gold films can withstand high temperature baking without the occurrence of excessive recrystallization.

This interferometer configuration acts in a manner similar to a retroreflecting mirror, and alignment is a simple task; however, the reflected light consists of a set of circular interference fringes that either expand or contract from the center as the substrate is deformed depending upon the tensile or compressive nature of the film stress. A single silicon detector mounted in the center of the return fringe pattern enables not only the amount of deflection to be measured but also allows the direction of motion to be determined automatically from the fringe change recording.

Since the separation of the base of the cat's-eye lens and the deforming substrate is limited in practice to a few hundred micrometers, thermal expansion of the lens and substrate mount do not introduce serious fringe count errors. For small separations between the two mirror surfaces the effect of an angular change ($\Delta\theta$) of the substrate is extremely small amounting to a change in optical path between the two apparent point sources of OPD = $D(\Delta\theta)^2/2$, where D is the separation between mirror surfaces. This insensitivity to angular tilts can be visualized if the distance between the mirrors is made negligibly small; when this occurs the two spherical waves reflected from both mirror surfaces slide inside one another and produce lateral shearing but no change in fringe patterns. In a similar manner, small changes in incident angles of the laser beam cause only a minute shearing of the component wavefronts that form the output fringe pattern.

The cat's-eye interferometer lenses used during the program were fabricated from Suprasil II and antireflection coated on the convex surface for 6328 Å. The flexible substrates of various thicknesses utilized during the program were fabricated from Cer-Vit, fused silica, KCl, germanium, zinc sulphide and zinc selenide. Thicknesses of 0.25, 0.5, 0.75 and 1.0 mm were used for the Cer-Vit and fused silica substrates, whereas 1.0-mm thick disks of the other materials were used because of the difficulty of polishing thin sections of these materials. Various spacers were fabricated for these different thicknesses to maintain a constant separation between the two reflecting surfaces and thus provide an output fringe pattern of uniform size at the detector.

The interferometer is illuminated with a 4-mm diameter collimated laser beam (6328 Å) produced by the interferometer laser source illustrated in Figure 2. The polarized beam from a 2-mW He-Ne laser is chopped by a synchronous chopper wheel and expanded to 4-mm diameter by a beam expander and spatial filter. A polarizing beamsplitter reflects approximately 1 percent of the "p" polarized laser beam to a silicon synchronous reference detector and

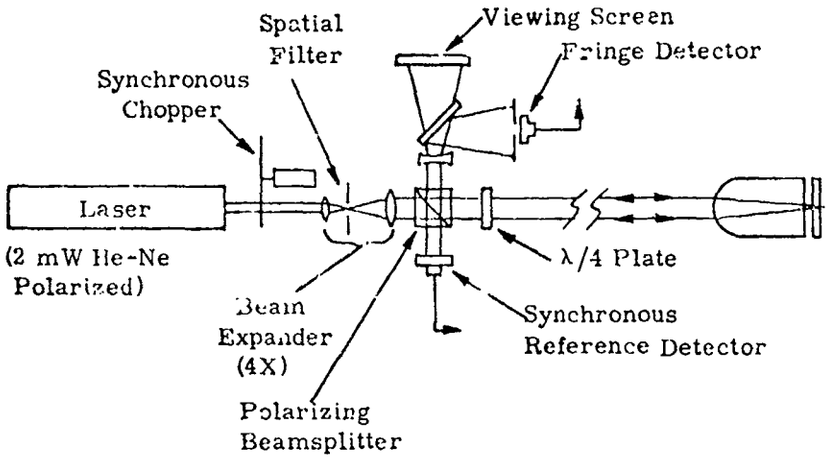

(a) Stress Interferometer Configuration

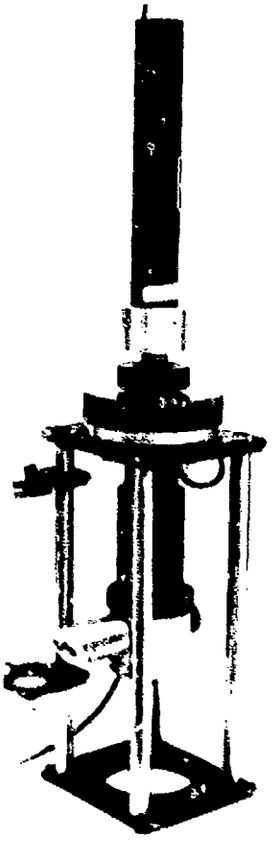

(b) Laser Interferometer Source

Figure 2. Stress Interferometer

transmits the remaining energy to the cat's-eye interferometer. A quarter-wave plate located between the polarizing beamsplitter and interferometer rotates the polarization from "p" to "s" after two passes, and the return fringe pattern is reflected by the polarizing beamsplitter to a fringe-count detector and display screen. The polarizing beamsplitter/quarter-wave plate system is used only to maximize the amount of light on the viewing screen and is not fundamental to the operation of the interferometer system.

2.3.1 Interferometer Configuration for Variable Vapor-Incidence Angles

Since stress levels in deposited films of certain materials are known to change with vapor-incidence angle, it is desirable to configure the interferometers inside the chamber such that four different vapor-incidence angles can be accommodated with minimal interferometer realignment. The addition of two small fold mirrors to the interferometer mount, together with an offset in angle of the cat's-eye interferometer such that its axis passes through the vapor source, allows incidence angles to be easily changed. Figure 3(a) illustrates this configuration and Figure 3(b) shows a photograph of an interferometer head.

The vapor-incidence angles attainable with either an electron-gun or resistance source located in the center of the chamber are variable at each interferometer between 0° and 42° with the existing tooling. The four positions allocated for rigid substrates are positioned on the same radius as the interferometer heads, and the vapor-incidence angles of the rigid substrate can also be set to any angle between 0° and 42°.

An optical-thickness monitor is located on the centerline of the chamber, and optical film thicknesses are monitored at any desired wavelength up to 1.0 μm by suitable choice of line filters. Optical thicknesses of the composite films of multilayers are individually monitored using fresh glass microscope slides for component films during an evaporation cycle.

The entire assembly of interferometers, rigid substrate holders, and optical monitor slides are enclosed in stainless-steel shields and can be heated to 250°C by a Calrod heater located at the top of the vacuum chamber (Figures 4(a) and (b)). Temperature control is obtained using an SCR proportional controller and thermistor mounted close to the interferometer housings.

2.3.2 Data Acquisition and Data Recording System

Stress changes in the films during deposition cause the bull's-eye fringe patterns at the fringe-count detector to expand or contract depending upon the nature of the stress (tensile or compressive). Changes in intensity of the central fringe are detected by PIN diodes and are fed to lock-in amplifiers that synchronously demodulate the chopped signals using a reference signal from a second silicon diode in the laser source housing.

The outputs of the optical monitor and stress interferometers are recorded on a six-channel chart recorder and are also applied to the input of a data-logger/punched tape recorder. Figure 5(a) and (b) illustrates the function and form of the data recording system.

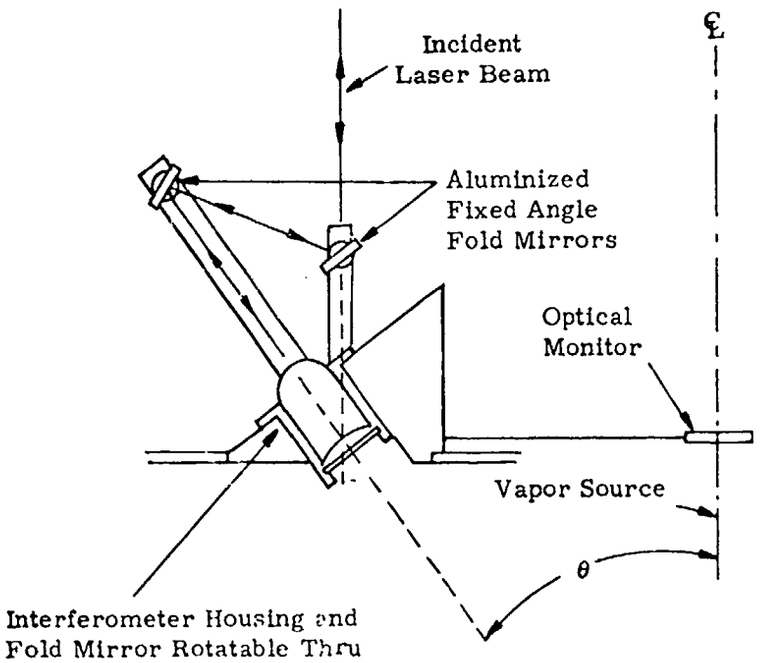

(a) Configuration

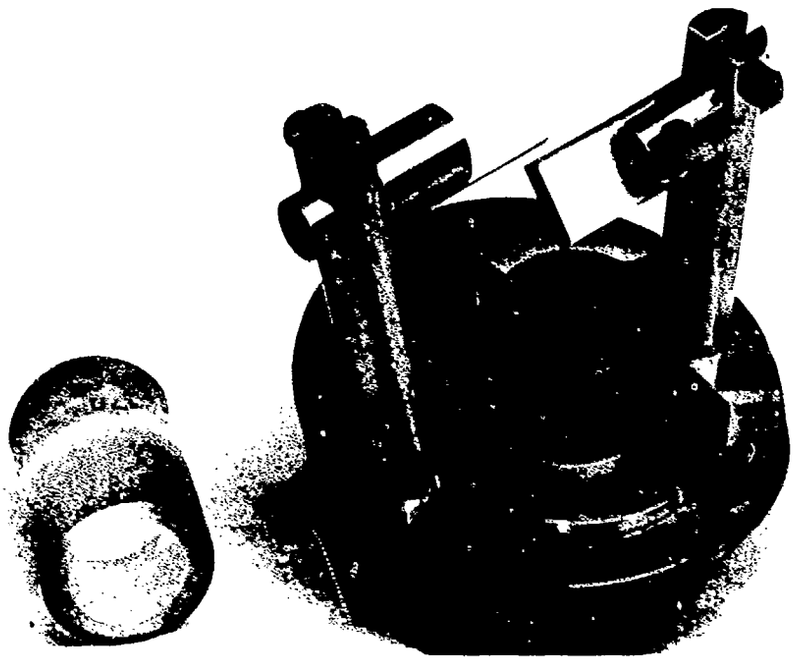

(b) Stress Interferometer Head with Variable Vapor-Incidence Angle Fold Mirrors

Figure 3. Variable Vapor-Incidence Angle Configuration

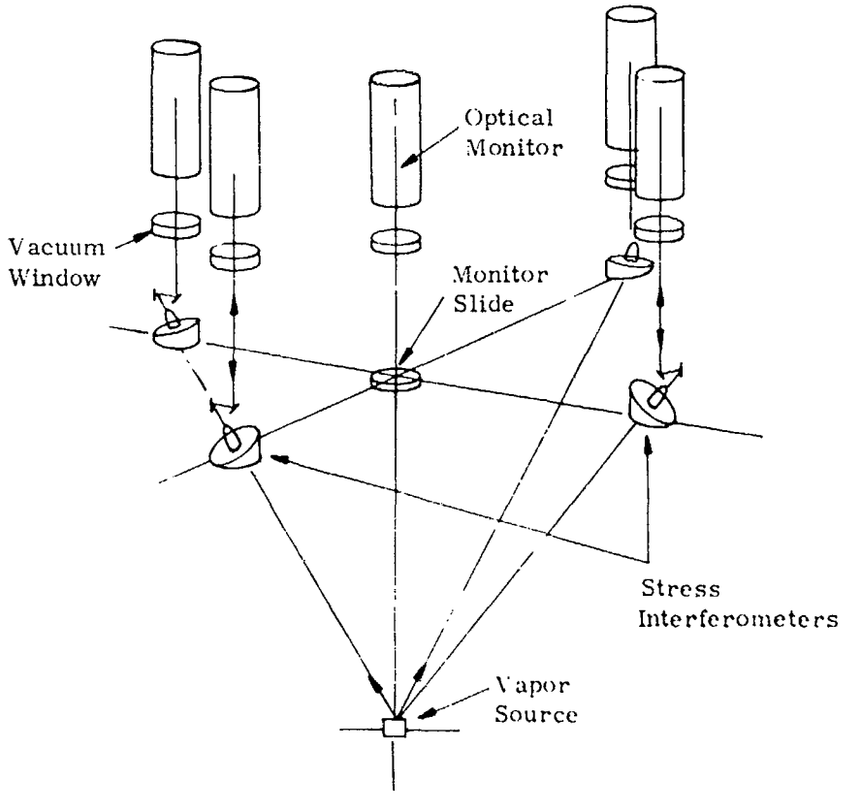

(a) Interferometer and Optical Monitor Configuration in a Vacuum System

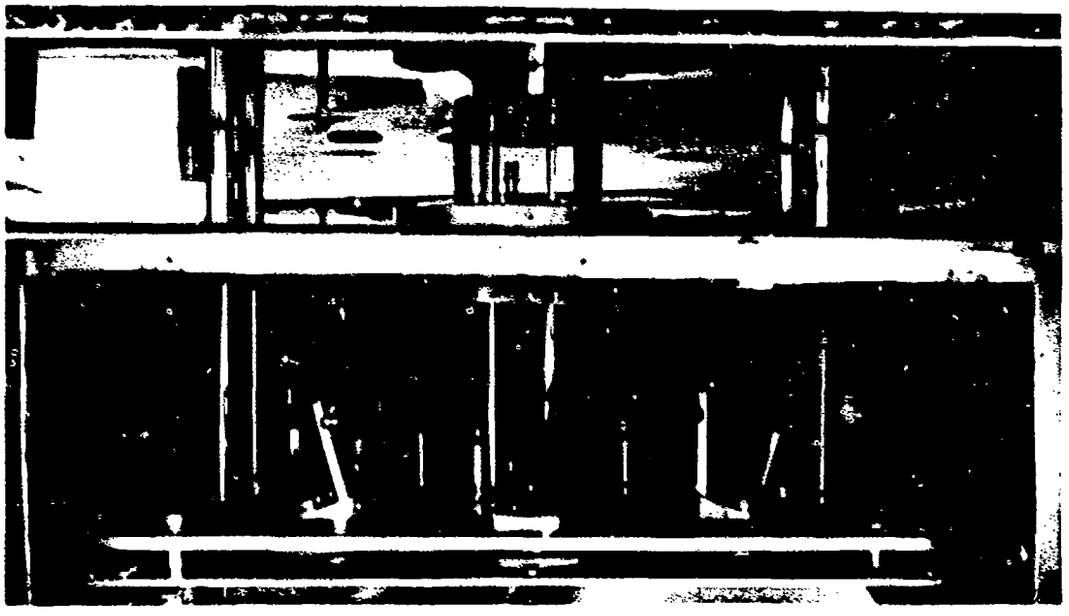

(b) Stress-Interferometer Array Inside Heated Enclosure

Figure 4. Stress Interferometer Array

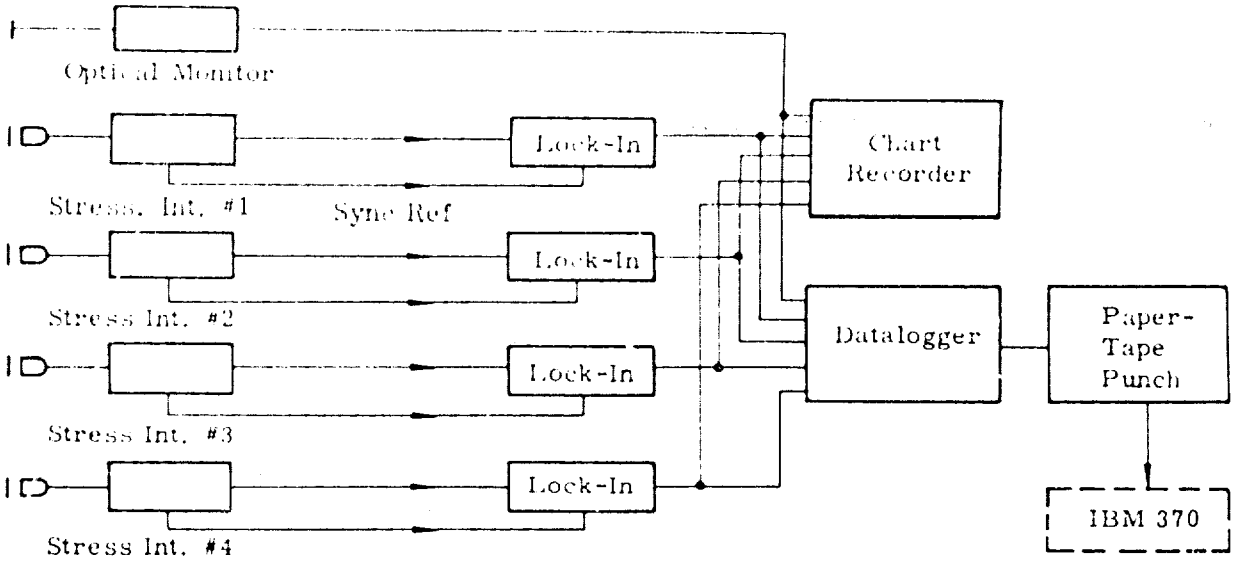

(a) Interferometer Data Acquisition and Recording System

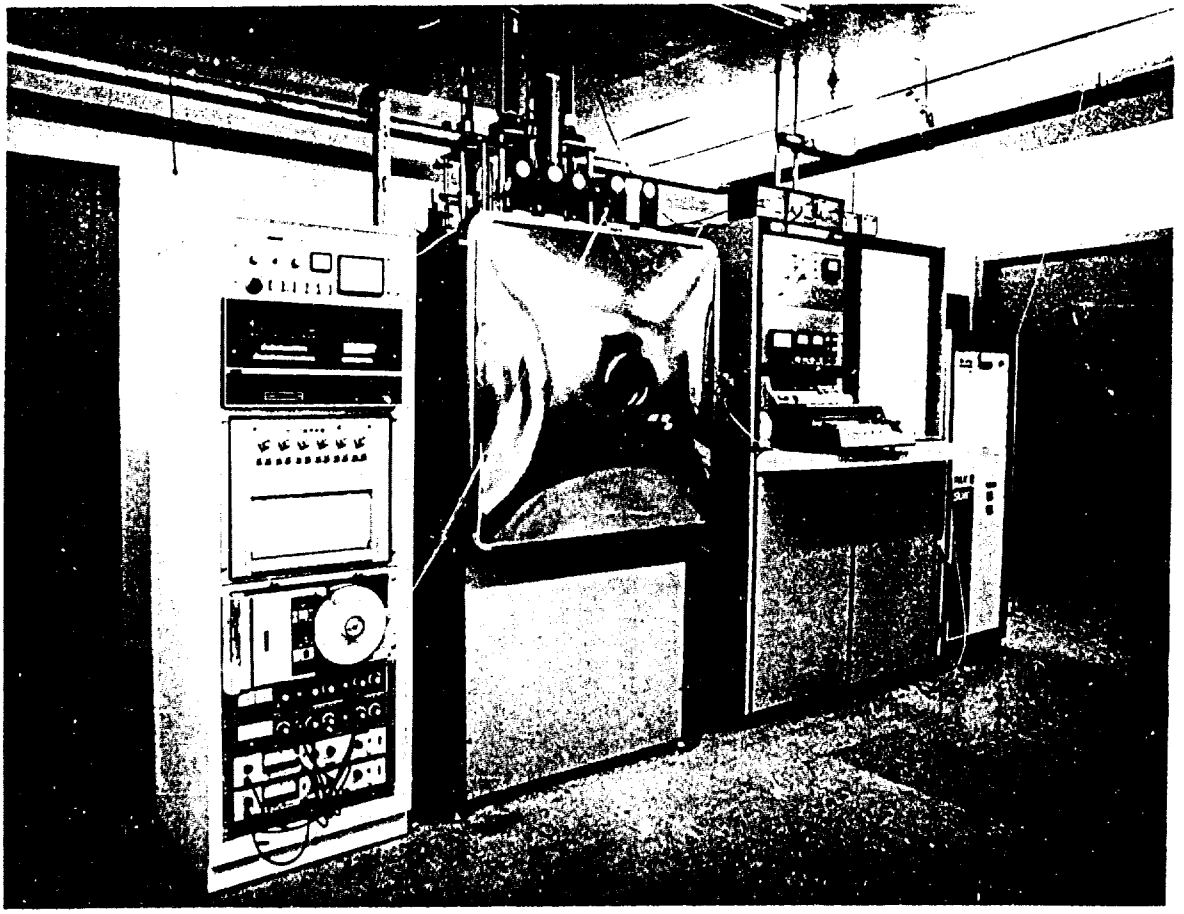

(b) Stress-Measuring Interferometer System with Data Recording Instrumentation

Figure 5. Data Acquisition and Data Recording System

The recording system data logger can be arranged to scan the five input channels at two fixed speeds of two channels/second or seven channels/second, the first channel always being the elapsed time. These two speeds in combination with the use of different glass thicknesses for the flexible substrate allow sufficient sampled data points to be recorded per fringe over a wide range of stress levels.

2.4 STRESS-MEASUREMENT SYSTEM - OPERATIONAL CHARACTERISTICS

Initial tests of a single stress interferometer mounted to the vacuum system showed that:

- Stable bull's-eye fringes were formed at the display screen and fringe-count detector, and pump vibration was not a disturbing factor.
- High contrast interference fringes are projected onto the detector, and changes in the fringes are recorded with great fidelity.
- Although heating the vacuum system to 250°C causes the fringe count to change because of nonuniform heating of the glass disk, the fringe system is reproducible and stable and of high contrast when the system reaches thermal equilibrium.

Figure 6 shows a typical fringe pattern (overexposed) produced at the detector (PIN-10 diode) and display screen; the detector's sensitive area is aligned with the center of the fringe pattern and detects intensity changes as fringes move away from or toward the center of the fringe pattern. Figure 7 shows the change in intensity or fringe count for a thin glass disk 0.25 mm thick at 200°C being coated with thorium fluoride evaporated from an electron-gun source. The fringe change contains an amplitude modulation due to material being deposited onto the second surface of the flexible disk. The use of a gold semitransparent film to provide a reflectivity of 50% at 6328 Å on the upper surface of the flexible disk, together with the 50% reference reflector, forms a three-mirror cavity and leads to amplitude modulation in the reflected fringes because of the deposited film thickness. Although this could be used to measure the deposited film thickness, it is not used in practice since the fringe counts obtained for thicker glass slides are generally of longer period than the optical thickness changes.

2.5 FRINGE DIRECTION SENSING USING A SINGLE DETECTOR

Sensing the direction of fringe motion during film deposition determines the sign of the stress, i.e., compressive or tensile. This information can be obtained either by observing the direction of fringe change during deposition or by the use of two detectors displaced laterally in the fringe pattern.

During initial testing of the cat's-eye interferometer, it was noted that the waveform generated by the detector as the fringes were either contracting or expanding possessed an asymmetry that occurred each cycle and depended upon the direction of fringe motion. This effect has since proven to be extremely useful since both the direction and magnitude of the stress are recorded automatically during deposition. Figure 8 illustrates this behavior

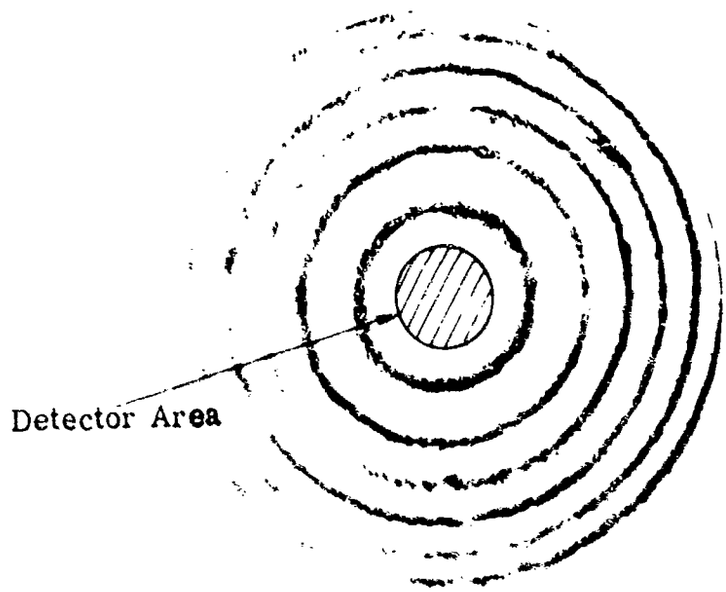

Figure 6. Fringe Pattern at Output of Stress-Measuring Interferometer

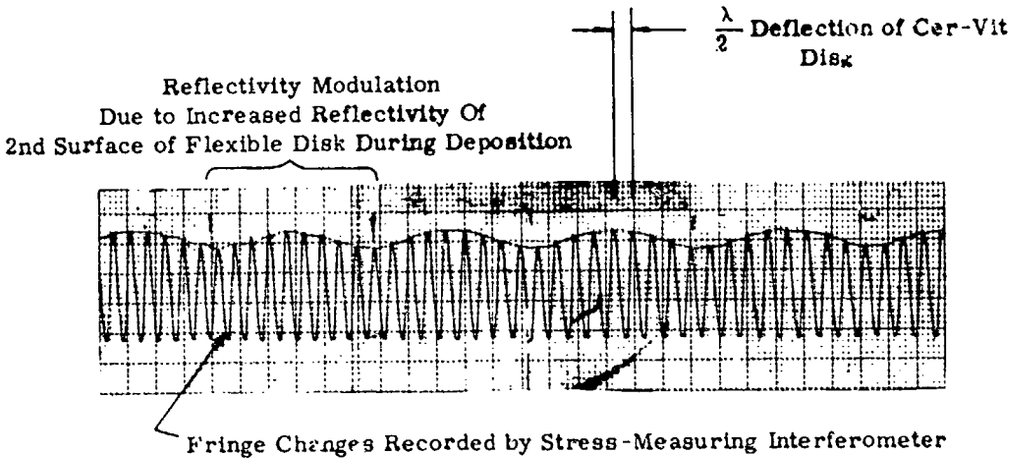

Figure 7. Intensity Variations (Fringe Count Due to ThF_4 Film Being Deposited onto a 0.25-mm Cer-Vit Disk)

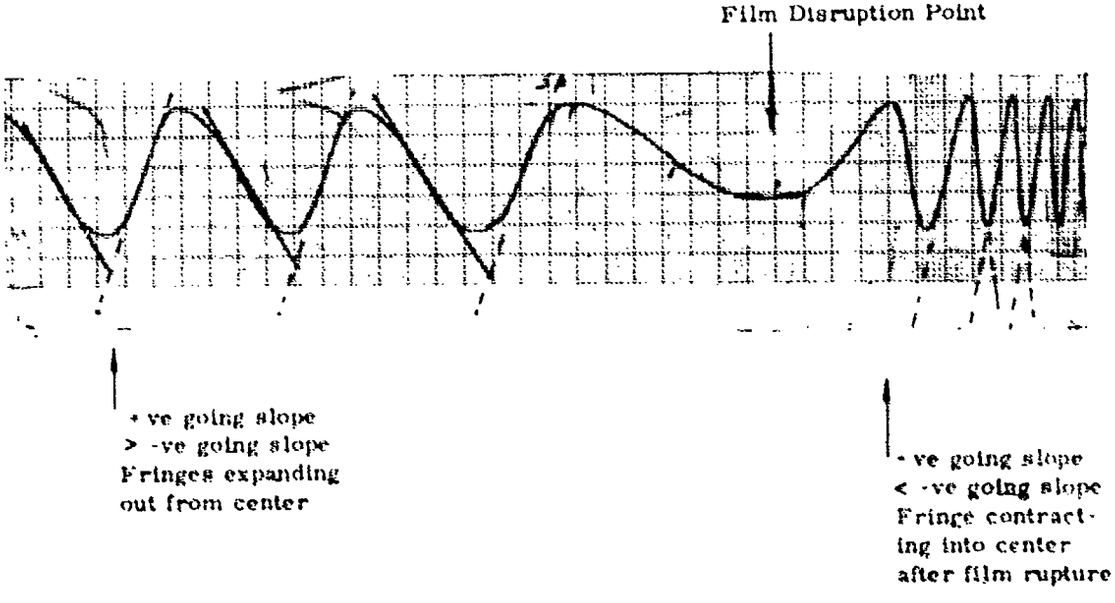

Figure 8. Fringe Count for a 0.5-mm Thick Cer-Vit Disk During Deposition of MgF_2 (Note waveform asymmetry indicating direction of fringe motion before and after film cracking)

for a film of magnesium fluoride deposited onto Cer-Vit at room temperature. As the film thickness increases from zero, the positive-going slope is greater than the negative-going slope, corresponding both to fringes moving outwards from the center of the fringe pattern and to a tensile stress. At the point indicated, the film breaks and the deflection reverses in sign; the fringes collapse into the center of the pattern; and stress-relief occurs corresponding to a stress reduction in the film. After film rupture, the positive-going slope is less than the negative-going slope, and this slope change with fringe direction can be utilized during data reduction to obtain the nature (sign) of the stress in the depositing film.

The asymmetry of the output waveform is not due to angular alignment errors in the fringe pattern and detector system but is quite reproducible and is a basic property of the interferometer configuration. The asymmetrical behavior arises from the interference of multiply reflected Gaussian beams which undergo radial shearing as the mirror separation alters. The fringe formation process was investigated theoretically for this interferometer (see Appendix A) by summing the first ten multiple reflections that occur between the two mirror surfaces. Gaussian intensity profiles were assumed for the reflected laser beams and the integrated energy falling on a detector of a given diameter was evaluated numerically as a function of the mirror separation. Figure 9 shows the computed detector signal as the mirror spacing is altered for two cases:

(1) A small detector diameter ~ 0.01 mm corresponding to operation of the interferometer in collimated light

(2) A detector area comparable to the beam size at the exit plane of the interferometer

The curves show the waveforms for a mirror separation change of $\lambda/2$ when the two reflectors are spaced 100 and 400 μm apart. The asymmetry is much more pronounced for large separations corresponding to reduced overlap of the reflected wavefronts. In practice, the mirror separation is of the order of 400 μm and the amount of asymmetry present in a recording of the fringe changes matches that predicted by analysis.

2.6 FILM STRESS DATA REDUCTION

Initial tests of the four-channel interferometer system showed that a stable and reproducible fringe count is obtained when the interferometers are mounted on the vacuum system. Vibration is not a problem and, although fringe changes occur during heating and cooling of the system, the changes in fringe count at constant high temperatures are small compared with the deflection caused by film stress. Thermal drifts at constant temperature when the system has reached equilibrium produce apparent stress errors of the order of 20 to 50 kg/cm^2 compared with expected material stresses of up to 5000 kg/cm^2. Figure 10 shows the chart recording obtained for a typical stress measurement experiment in which thorium fluoride was deposited onto Cer-Vit disks of various thicknesses at 200°C. The fringe changes caused by film stress are recorded on channels 1, 3, 4 and 5, while channel 2 contains a recording from the optical monitor located in the center of the chamber. All these waveforms are recorded on paper tape via a data-logging system and the sampled data are processed using an IBM 370 after the deposition is completed.

$$I = 2\pi \int_{o}^{R_{eo}} \frac{2P}{\pi} \left(\sum_{1} P_1 \exp(a_i + jb_i) \right) \times \left(\sum_{1}^{n} P_i \exp(a_i + jb_i) \right) rdr$$

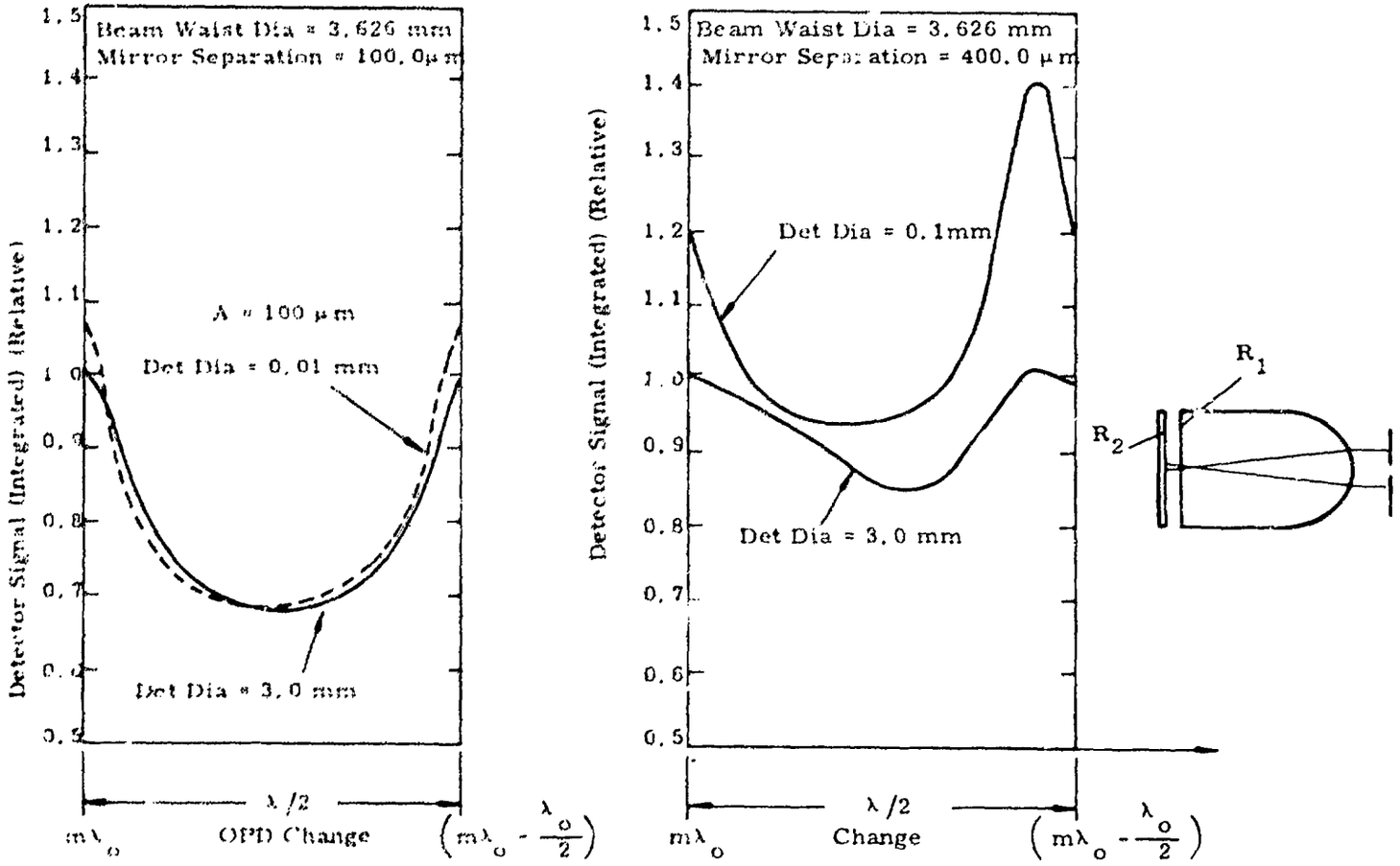

Note: Relative Phase Shifts Between Curves Have Been Subtracted to Show Maxima at Same Position

Figure 9. Computer Waveform Asymmetry for Cat's Eye Interferometer

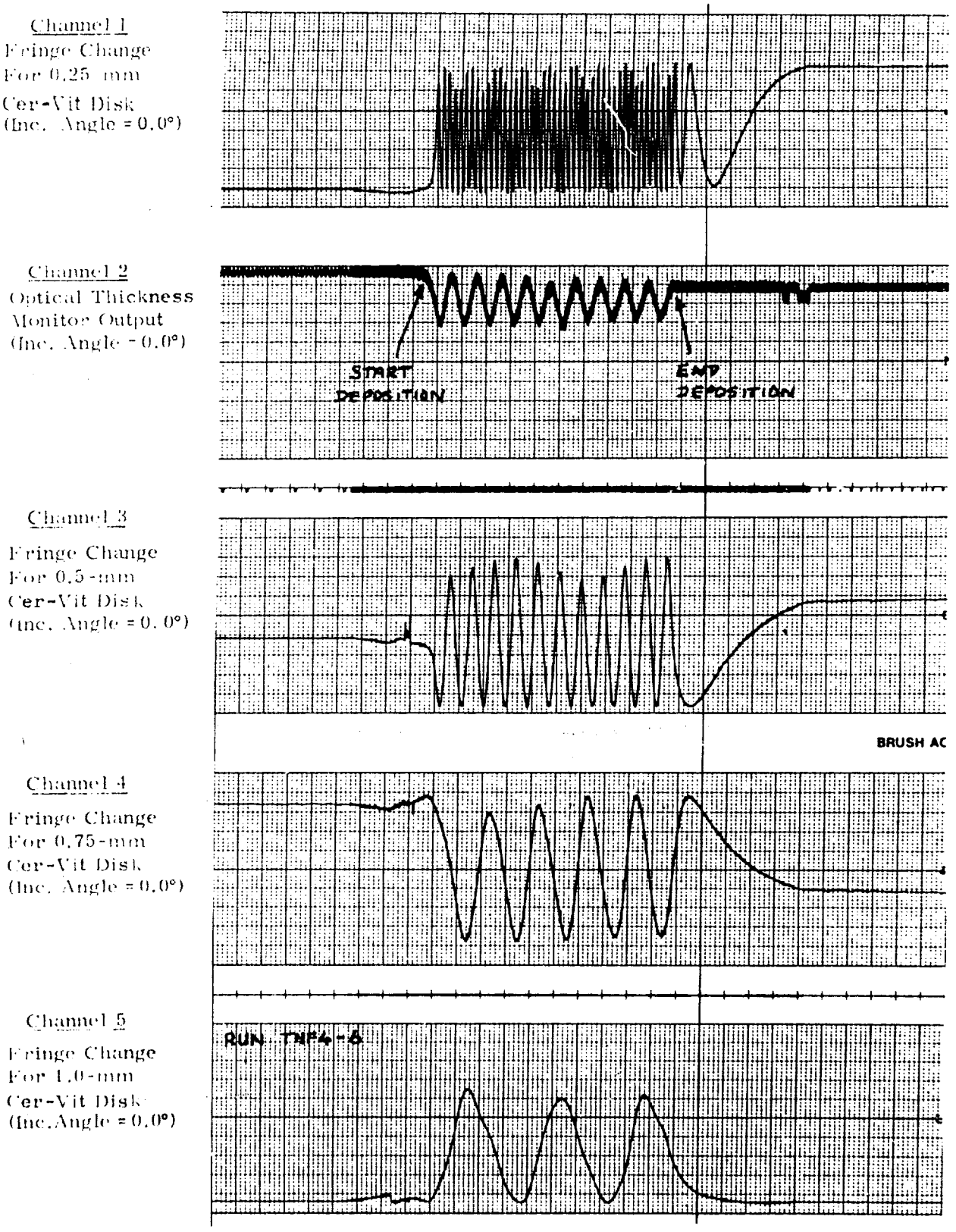

Figure 10. Data Recording for Four Simultaneous Stress Measurements for ThF_4 Deposited onto Cer-Vit Disks of Varying Thicknesses at 200°C

The total number of sampled data points per channel is nominally 250 (data rate of two channels/second) for the entire deposition run, but this can be varied by changing the recording speed and/or the glass disk thickness. This number of data points is typical for the deposition of $\lambda/4$ films at 10.6 μm, although a data rate of seven channels per second is available from the data-logger/tape-punch unit.

The recorded data is processed to yield the stress in the film deposited onto each disk, and the data reduction calculates the average stress $\langle S_i \rangle$ for the i^{th} disk according to

$$S_i = \frac{4E_i w_i}{3(1-\nu_i)} \left(\frac{h_i}{D_i}\right)^2 \frac{1}{t_m \delta_i} \qquad (1)$$

where

E_i = Young's modulus of i^{th} disk

ν_i = Poisson's ratio of i^{th} disk

h_i = Thickness of i^{th} disk (mm)

D_i = Diameter of i^{th} disk (mm)

w_i = Deflection due to stress $\langle S_i \rangle$ of i^{th} disk (μm)

t_m = Mechanical thickness of film deposited on monitor slide

δ_i = Distribution factor for i^{th} slide (ratio of thickness on the i^{th} slide to thickness of film on the optical monitor)

The deflections (w_i) are obtained from the sample data by the following algorithm:

(1) Normalize all channels to the maximum recording occurring during deposition.

(2) Locate zero crossing points.

(3) Normalize individual cycles to unity.

(4) Calculate mechanical deflections.

(5) Differentiate deflections and sum absolute values.

The mechanical thickness of the film deposited onto the optical monitor is also calculated in a similar manner and, together with the distribution factors (δ_i) and the optical deflections (w_i), is used to calculate the average stress $\langle S_i \rangle$ for each point recorded. The data computed in this manner are interpolated to provide stress level as a function of the mechanical film thickness deposited onto each substrate. Figure 11 shows the data reduction

STRESS DATA ANALYSIS

RUN 30 11 DEC 22 THF4 200C 0.25,0.5,0.75,1.0 PM CHRVIT /CH2/SEC

F[illegible] NAME = THF4-6

INPUT DATA LISTED

	CHANNEL 1	CHANNEL 2	CHANNEL 3	CHANNEL 4	CHANNEL 5
RAW DC VOLTAGE	7.504	0.093	7.496	0.693	0.552
REF DC VOLTAGE	0.770	0.066	0.259	0.131	0.094

SUBSTRATE PARAMETERS

	CHANNEL 1	CHANNEL 2	CHANNEL 3	CHANNEL 4	CHANNEL 5
SUB MATERIAL	1		1	1	1
WEIGHT (GMS)	0.324		0.616	0.983	1.295
SUB THICKNESS (CM)	0.256		0.486	0.775	1.022
DIST(COS) FACTOR	0.733		0.693	0.712	0.761

***** FILM DEPOSITED = 20 QUARTER WAVES OF INDEX 1.48 AT 0.604 MICRONS *****

SUBSTRATE DEFLECTION (MICRONS)
(CHANNEL 2 IS OPTICAL MONITOR)

CHANNEL 1	CHANNEL 2	CHANNEL 3	CHANNEL 4	CHANNEL 5
0.029	0.016	0.000	0.001	0.0
0.128	0.085	0.014	0.053	0.026
0.530	0.239	0.098	0.077	0.053
0.949	0.334	0.234	0.100	0.077
1.424	0.425	0.338	0.131	0.102
1.848	0.562	0.432	0.174	0.142
2.277	0.630	0.571	0.221	0.200
2.750	0.732	0.669	0.269	0.230
3.164	0.849	0.771	0.329	0.251
3.639	0.963	0.905	0.397	0.267
4.075	1.065	1.004	0.424	0.278
4.527	1.159	1.119	0.464	0.314
4.965	1.294	1.245	0.506	0.333
5.407	1.439	1.335	0.566	0.369
5.896	1.529	1.471	0.628	0.408
6.326	1.619	1.579	0.692	0.439
6.777	1.789	1.677	0.734	0.472
7.211	1.869	1.810	0.769	0.499
7.641	1.969	1.911	0.809	0.528
8.113	2.113	2.008	0.864	0.575
8.543	2.207	2.152	0.927	0.606
9.017	2.316	2.250	0.997	0.631
9.450	2.389	2.351	1.042	0.649
9.903	2.500	2.496	1.083	0.670
10.366	2.644	2.589	1.124	0.702
10.794	2.726	2.700	1.169	0.729
11.274	2.845	2.836	1.229	0.753
11.707	3.047	2.934	1.296	0.784
12.181	3.162	3.065	1.348	0.826
12.616	3.305	3.176	1.393	0.844
13.062	3.416	3.260	1.434	0.866
13.527	3.489	3.421	1.455	0.881
TOTAL NO OF MAX AND MINIMA	89	43	22	11	6
DEPOSITION RATE (A/SEC)	33.298	45.120	31.259	32.125	34.341

STRESS DATA REDUCTION

STRESS LEVEL 200/CM.CM CHANNEL 1	FILM THICKNESS (MICRONS) CHANNEL 2	STRESS LEVEL [illegible] CHANNEL 3	STRESS LEVEL [illegible] CHANNEL 4	STRESS LEVEL [illegible] CHANNEL 5
[illegible]	0.[illegible]	[illegible]	[illegible]	[illegible]
[illegible]	0.[illegible]	[illegible]	[illegible]	[illegible]
[illegible]	0.[illegible]	[illegible]	[illegible]	[illegible]
1063.094	0.400	1019.849	1017.335	1415.[illegible]
1062.796	0.500	1030.502	1041.425	1393.[illegible]
1119.274	0.600	1076.329	1126.196	1[illegible].927
1111.544	0.700	1083.363	1097.827	1197.[illegible]
1101.019	0.800	1092.045	1104.713	1197.829
1125.314	0.900	1061.014	1154.920	1204.663
1099.402	1.000	1079.173	1137.699	1187.240
1114.111	1.100	1074.864	1127.648	1202.[illegible]
1118.224	1.200	1099.[illegible]	1150.741	1243.[illegible]
1126.413	1.300	1102.[illegible]	1200.709	1237.[illegible]
1145.705	1.400	1111.[illegible]	1202.299	1219.[illegible]
1140.140	1.500	1104.[illegible]	1190.470	1210.[illegible]
1141.023	1.600	1094.963	1200.669	1200.[illegible]
1133.669	1.700	1086.213	1179.990	1183.[illegible]
1121.910	1.800	1076.699	1172.[illegible]03	1190.[illegible]
1119.084	1.900	1104.907	1163.361	1171.[illegible]
1129.842	2.000	1098.263	1152.021	1134.[illegible]

Figure 11. Stress Data Reduction of Data in Figure 10, ThF_4-6 Deposited onto Substrates of Various Thicknesses at 200°C

for the curves shown in Figure 10 for a thorium fluoride film deposited onto Cer-Vit disks of various thicknesses. Evaporation rates are automatically calculated for each channel together with the number of fringes calculated by the data-reduction program and serve as a check on the experimental conditions. The optical monitor input from the Balzer monitor is an extremely noisy signal resulting in double maxima and minima when depositing ThF_4 on 1.5 index monitor slides and, consequently, the fringe count for channel 2 is computed incorrectly as are the variations of thickness with time. Since the noise is uniform throughout the recording and since the optical film thickness is deposited as an exact number of quarter-waves at some preselected monitor wavelength, the thickness data is linearly scaled to the correct thickness. This source of error was subsequently eliminated by depositing ThF_4 films onto high-index monitor slides.

The entire interferometer system was used for a series of preliminary experiments designed to check out the entire system under operational conditions, and thorium fluoride (ThF_4) was selected as the thin-film material because of its wide use in laser coatings in the 10-μm region.

2.7 EVALUATION OF STRESS MEASURING SYSTEM - EXPERIMENTAL TESTS

The calculation of stress utilizing equation (1) assumes that:

(1) The deposited film thicknesses are small compared to the flexible substrate thickness

(2) The measurement is independent of the substrate material chosen

(3) The measurement is independent of the substrate thickness

(4) No stress relief occurs in the substrate/film combination and no slippage occurs at the film/substrate boundary.

The first condition is satisfied for $\lambda/4$ films in the 10-μm region (t = 1 to 2 μm) as described here since the flexible glass substrates used range from 250 to 1000 μm in thickness. The dependence, if any, of the stress measurement upon the thickness and type of substrate material used can be checked using the present four-channel interferometer system. The final condition is more difficult to verify experimentally, but calculations given in Section 3 show that the effects of stress relief are small for thick films. Since the interferometer system can measure the stress on four different thicknesses of materials or on different substrates in the same vacuum deposition, the second and third conditions can be checked experimentally.

The data shown in Figures 10 and 11 give the stress levels for ThF_4 films deposited onto Cer-Vit disks of different thicknesses of known weight and density and show that indeed the equilibrium stress is independent of the glass substrate thickness. A similar experiment was carried out utilizing thin flexible disks of fused silica, Cer-Vit and potassium chloride to determine the effect of different substrate materials. The disk thicknesses were obtained by weighing the disks, and the elastic constants for each material used in the data reduction are shown in Table 1.

TABLE 1. MECHANICAL PROPERTIES OF FLEXIBLE SUBSTRATES

Material	Young's Modulus (E)	Density	Poisson's Ratio (ν)
Cer-Vit*	9.23×10^5 kg/cm^2	2.5 g/cm^3	0.25
Fused Silica**	7.00×10^5 kg/cm^2	2.2 g/cm^3	0.17
KCl (Ref. 9)	3.02×10^5 kg/cm^2	1.98 g/cm^3	0.11

*Owens-Illinois Data
**Corning Glass Works Data

The stress data measured for ThF_4 using two KCl substrates (1.0 mm thick), a 0.5-mm thick fused silica substrate and a 0.5-mm thick Cer-Vit substrate are shown in Figure 12.

These intrinsic stress levels measured for ThF_4 agree within 10% for different substrate materials although subsequent measurements of ZnSe films on various substrates showed wide discrepancies for Cer-Vit and KCl substrates. Whether the intrinsic stress is truly dependent upon the substrate material or whether the high expansion substrate (KCl) in combination with a film of high index cause enhanced thermal deflections is not known.

9. L.S. Combes, S.S. Ballard, and K.A. McCarthy, J. Opt. Soc. Amer., 41, 215 (1951).

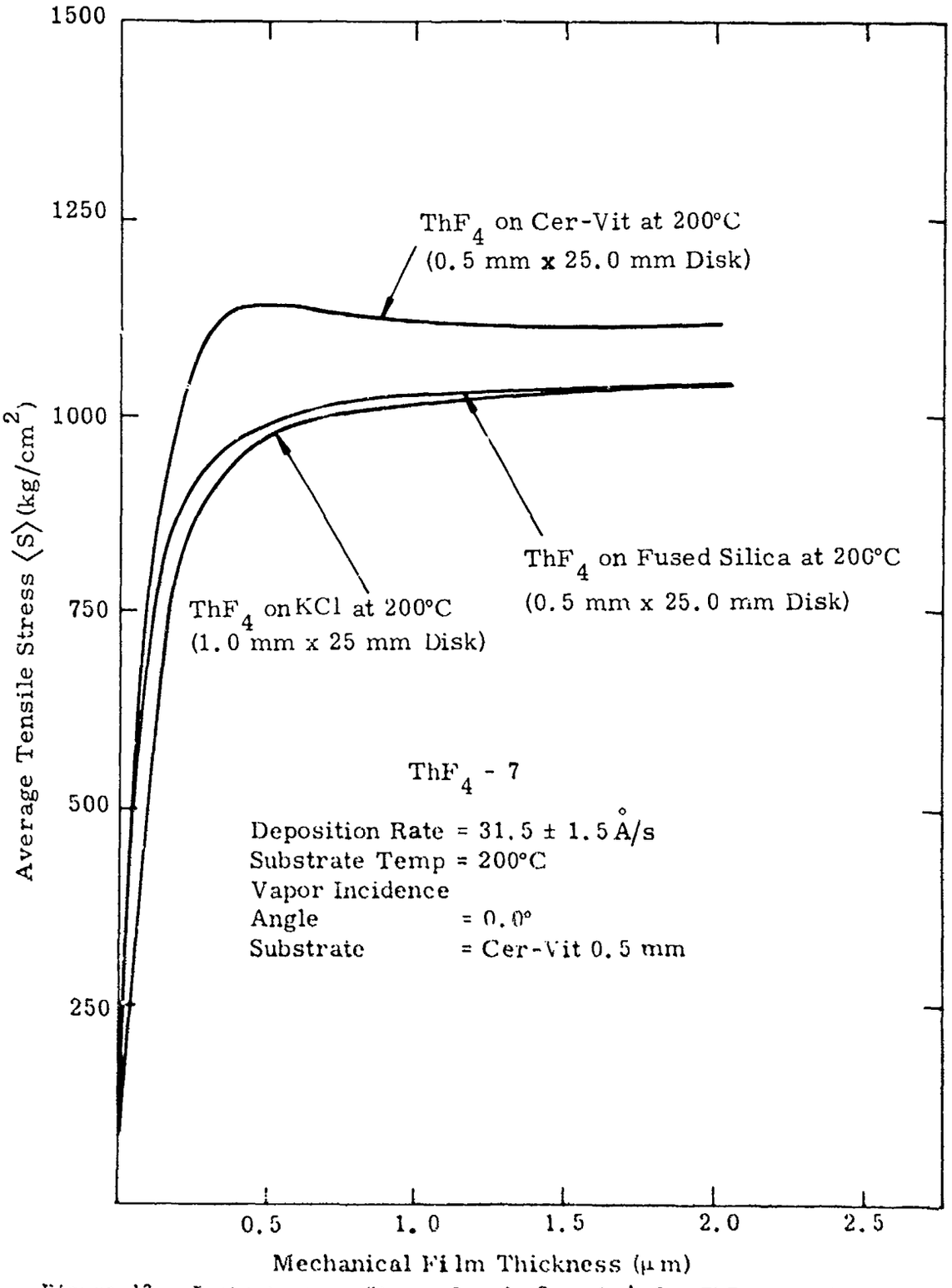

Figure 12. Instantaneous Stress Levels Computed for ThF_4 Deposited onto Cer-Vit Fused Silica and KCl under Identical Conditions.

SECTION 3

STRESS ADDITION AND TEMPERATURE EFFECTS IN THIN FILM MULTILAYERS

3.1 ANALYTICAL MODEL FORMULATION

An analytical task was undertaken as part of this program to model the stress behavior of multilayer film stacks in order to identify modes of failure when exposed to intense laser beams.

Such a model requires at the very least experimentally measured data of intrinsic film stresses, thin-film thermal and mechanical properties, disruptive film thicknesses, adhesion and film breaking stresses. A knowledge of such properties for the component materials of a thin-film stack should in principle enable the spatial stress distribution within each film to be computed when the coating is placed in a spatially nonuniform high energy laser beam. Predicting the stress levels at which a film system fails involves measurement of both film adhesion and the breaking stress level; and such measurements have always proven difficult since models of film adhesion are virtually non-existent.

The present effort is aimed principally at providing a better understanding of antireflection coatings deposited onto window materials that have large thermal expansion coefficients. Window materials such as potassium chloride, calcium fluoride and strontium fluoride are extensively utilized for CO_2 lasers and chemical lasers, and all possess much higher expansion coefficients than most materials traditionally utilized for antireflection coatings in the infrared region.

As a starting point for this topic it is instructive to describe the behavior of a thin disk upon which a stressed film is being deposited at high temperatures. Since film stress is obtained indirectly by measuring the deflection of a thin disk, such an analysis also quantifies sources of error in the measurement technique.

The substrates utilized for stress measurements consist of a thin glass disk whose upper surface is coated with a partially reflecting metal film, which itself can cause a deflection of the disk w_G due to its own internal film stress. When this disk is placed in the interferometer and heated by external sources (Calrod heaters, quartz iodine lamps, etc.), the disk distorts primarily because of the existence of radial and front to back temperature gradients producing deflections w_{R1} and w_{FTB1}, respectively. After equilibrium is established in the vacuum system, opening of shutters and exposure to a hot vapor source can introduce short-term temperature gradients that produce a deflection w_S at the start of evaporation. Such thermal deflections occur when film stress is low since films appear to approach zero stress at zero thickness, and this effect can introduce large errors in the measured stress. A continuous deflection occurs during deposition, the rate of deposition being proportional to the stress if the film thickness increases linearly. This deflection $w_f(t)$ is used to calculate the intrinsic film stress of the film

material knowing the elastic properties of the substrate. As the coated disk is cooled to room temperature after the film is deposited, deflections are caused by radial and front to back gradients ω_{R2} and ω_{FTB2} as during heating together with a deflection ω_{DTE} caused by any mismatch in thermal expansion of the film and substrate. The amount of deflection ω_{DTE} depends on both the expansion coefficient mismatch and the elastic properties of the film and substrate. A further deflection ω_{AIR} can occur when the substrate is exposed to air.

The deflection of the disk during these processes is the sum of all these effects, i.e.,

$$\omega = \omega_G + \omega_{R1} + \omega_{FTB1} + \omega_S + \omega_f(t) + \omega_{R2} + \omega_{FTB2} + \omega_{DTE} + \omega_{AIR} \qquad (2)$$

and the experimental conditions must deduce the deflection due to film stress $\omega_f(t)$ from the total deflection ω. The above expression pertains to a single film being deposited onto a flexible substrate. When multiple films are deposited at the same temperature, the deflection caused by the i^{th} film produces small stress changes in all the preceding films, a phenomenon we describe as stress relief. Fortunately, we will show that the stress changes caused by additional deformation of the substrate are exceedingly small and can be neglected when the total film thickness is much less than the substrate thickness. The deflection obtained for multiple films can be represented as a sum of the deflections due to the individual films, the intrinsic stress of all preceding films being unaffected by the addition of the i^{th} film at constant temperature.

Since the intrinsic stress for most film materials varies with thickness it is important to understand the relationship between unit stress $\sigma(t)$ and the stress calculated from the disk deflection equations $\langle S(t) \rangle$. The value $\langle S(t) \rangle$ is calculated from the total deflection of the disk ω at a particular film thickness and, as such, is a weighted average of the unit stresses $\sigma(t)$ of all the infinitesimally thin layers of thickness dt that form the growing film. When the unit stress in the material is constant, then $\sigma(t) = \langle S(t) \rangle$, but this is not the case for thin films since the measured stress tends toward zero at zero thicknesses. All of the experimental methods for stress measurement provide the weighted stress $\langle S(t) \rangle$; however, the unit stress $\sigma(t)$ is a more fundamental quantity for modeling the behavior of multilayer films and this function can be derived from the experimentally measured values of $\langle S(t) \rangle$ as will be shown.

The total deflection of the thin disk during film growth at a <u>constant temperature</u> is therefore the sum of the first five terms in equation (2), i.e.,

$$\omega = \omega_G + \omega_{R1} + \omega_{FTB1} + \omega_S + \omega_f(t)$$

In the experiments carried out during this program, the deflection due to the partially transparent gold film on the top surface of the substrate is assumed to be small and of constant value during film deposition. Similarly, since the thin disks are allowed to reach thermal equilibrium over a long time period, the deflections caused by radial and front to back gradients ω_{R1} and

ω_{FTB}, are assumed constant and small. This assumption is valid during a measurement since the change in fringe intensity due to such gradients is monitored during the heating cycle until the changes become negligibly small, of the order of one or two fringes per hour.

The time dependent disk deflection at constant temperature during deposition is therefore

$$\omega(t) = \omega_S(t) + \omega_f(t)$$

where $\omega_S(t)$ is the deflection caused by opening or closing the shutters located beneath the substrate and by exposing the disk surface to the hot vapor source either by opening a source shutter or by heating the evaporant material.

The contribution from the opening and closing of substrate shutters can be extremely large, especially if a film has been previously deposited onto the disk; however, these transients can be allowed to die away before film deposition is started. Thermal fluxes from the hot source material cannot be so conveniently minimized and can contribute large errors at the start of film deposition, where the intrinsic stress is changing most rapidly during the nucleation and island growth phase. A mathematical description of the behavior of an absorbing disk coated with a second surface gold reflector illuminated by a hot source was attempted during the program in order to estimate the amount of deflection expected for various sources and substrate materials. The resulting second-order inhomogeneous differential equation that is obtained must be evaluated numerically to obtain the temperature gradients in the disk and the corresponding time-dependent deflections. This analysis was not pursued since experimental measurements for uncoated thick disks utilized during the measurement program showed that such effects were small, amounting to an error of 100 kg/cm^2 at most for the various substrate materials used. A rigorous thermal analysis is still required for the case of a coated disk since thermal stresses due to expansion mismatch may produce large apparent stresses. These source-induced deflections were minimized by preheating the evaporant with the source shutter open, and evaporation was initiated by increasing the power to the electron beam gun.

Expressions are derived in the following paragraph for the various deflection contributions described above for a thin disk together with the relationship between the measured stress $\langle S(t) \rangle$ and the more fundamental unit stress $\sigma(t)$. The effect of stress relief is calculated and the influence of thermally induced stress due to expansion coefficient mismatch and thermal gradients are derived for a single film. The results are then utilized to describe the behavior of a multilayer coating under conditions of changing temperature.

3.2 DEFLECTION OF CIRCULAR PLATES DUE TO A SINGLE STRESSED FILM

Although the equation for the deflection of a thin disk due to a stressed coating has been derived by many authors, we include the derivation here for the sake of completeness. The equation for stress and deflection derived in the following discussion assumes that:

(1) The film properties are uniform; i.e., unit stress is uniform in a plane perpendicular to the direction of film growth

(2) The disk is stress-free and no twisting moments exist within the material or are induced in the disk by the deposition of a thin film of material; i.e., stress is isotropic

(3) Deflections are small compared with the substrate thickness

(4) No slippage occurs at the film substrate boundary.

If the circular plate has a thickness h and a diameter D, the initially unstressed disk is bent to a sphere by the film and the neutral surface of the disk assumes a sphericity r, as shown in Figure 13. The film shown in Figure 13 is under tensile stress, and the deflection, ω, of the neutral surface due to the film stress is for small deflections.

$$\omega = \frac{D^2}{8r} \tag{3}$$

The bending moment, M, and the disk radius, r, are related by (Ref. 10)

$$\frac{1}{r} = \frac{M}{A(1+\nu)} \tag{4}$$

where

$$A = \frac{Eh^3}{12(1-\nu^2)} \tag{5}$$

and

$$M = \int_{h/2}^{h/2+t} \sigma(z) z dz \tag{6}$$

Here the material parameters are

E = Young's modulus of elasticity

ν = Poisson's ratio

σ = Unit stress in the film (i.e., stress in a thin layer dz at distance z from the neutral surface)

Combining equations (3), (4), and (5), the deflection (ω) in terms of the induced bending moment, M, of equation (6) becomes

$$\omega = \frac{3}{2}\left(\frac{1-\nu}{E}\right)\left(\frac{D^2}{h^3}\right) M \tag{7}$$

10. S. Timoshenko, Theory of Plates and Shells, 2nd ed. (McGraw-Hill, New York, 1959) p. 43.

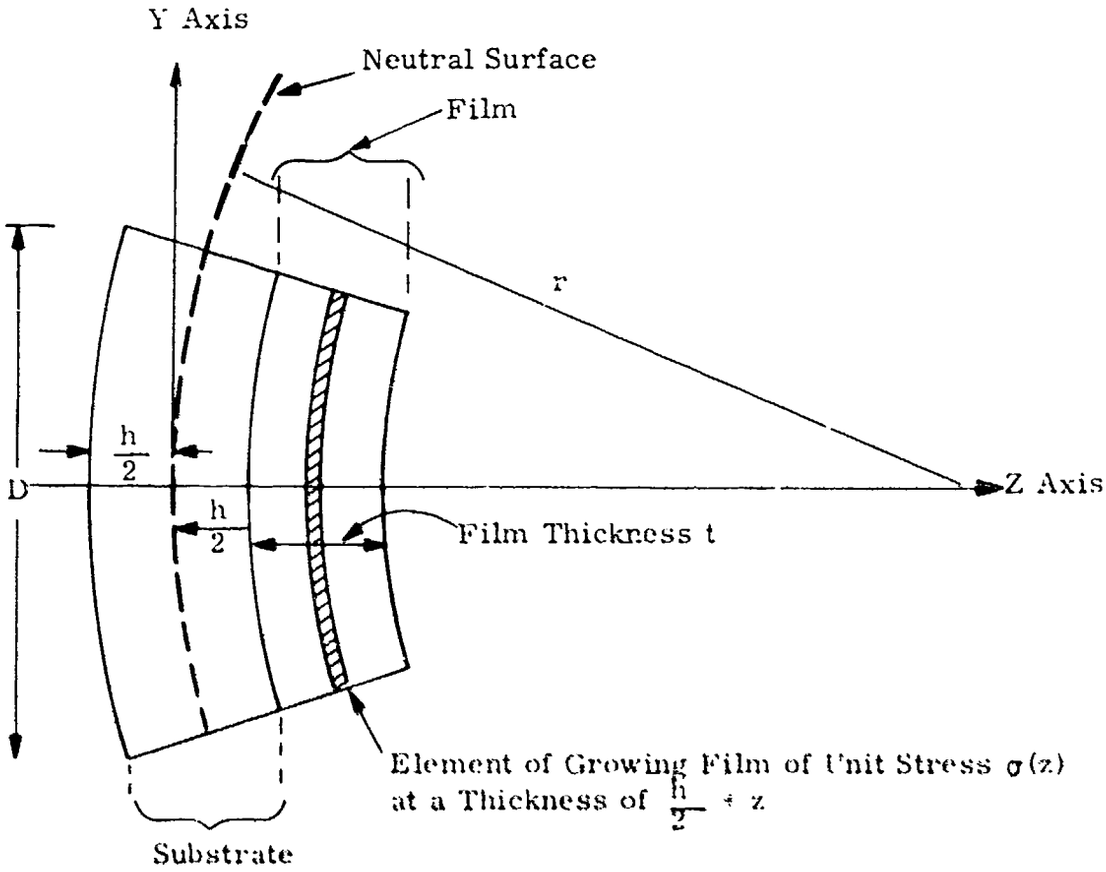

Figure 13. Deflection of Disk due to a Single Stressed Film

The stress measured during an experiment is the average stress, $\langle S \rangle$, and this value is a function of film thickness since the unit stress depends upon film thickness. The relationship between experimentally measured stress $\langle S \rangle$ and the unit stress $\sigma(z)$ can be obtained by considering the origin of the bending moment due to a film of thickness t at a distance h/2 from the neutral surface producing a deflection that is equivalent to the existence of an average stress $\langle S \rangle$ in the film a distance h/2 from the neutral surface, i.e.

$$M = \int_0^t \sigma(t)\ (h/2 + t)dt = h \langle S \rangle\ t/2 \tag{8}$$

The unit stress at any thickness can therefore be obtained from measured data as

$$\sigma(t) = \left(\frac{h}{h+2t}\right) \frac{d}{dt} \left\{ \langle S \rangle\ t \right\} \tag{9}$$

which for the case where $t \ll h/2$ reduces to the form

$$\sigma(t) = \langle S \rangle + t \frac{d}{dt} \langle S \rangle \tag{10}$$

Equation (7) can now be written as

$$w = \frac{3}{2} \left(\frac{1-\nu}{E}\right)\left(\frac{D^2}{h^3}\right) \int_{h/2}^{h/2+t} \sigma(t)\left(\frac{h}{2} + t\right) dt \tag{11}$$

$$= \frac{3}{2} \left(\frac{1-\nu}{E}\right)\left(\frac{D^2}{h^3}\right)\left(\frac{h}{2}\right) \langle S \rangle\ t \tag{12}$$

so that the average film stress measured at some thickness t is

$$\langle S \rangle = \frac{4E}{3(1-\nu)} \left(\frac{h}{D}\right)^2 \left(\frac{w}{t}\right) \tag{13}$$

If this function is continuously calculated during film deposition, the unit stress at any point in the film can be obtained from equation (10).

3.3 UNIT STRESS CURVE FITTING

A knowledge of the unit stress function for a given coating material completely describes its stress behavior and is utilized for calculating the deflection of a disk when coated with multiple films.

During the early portion of the program, the stress behavior of thorium fluoride was measured for different substrate temperature disposition rates and angles of incidence for film thicknesses up to 1.5 μm (see Section 4) and showed that the stress always approached a constant value as the film thickness increased. These equilibrium values were slightly different for the

various deposition conditions but the functional form of the stress variations were similar. Later measurements for zinc selenide and cerium fluoride showed a similar behavior with increasing film thickness although the rate at which the equilibrium value is reached is greatly different for each material under comparable evaporation conditions.

In order to characterize the materials in a convenient mathematical form, data points for the average stress were fitted to a polynomial by least squares methods

$$\langle S \rangle = \sum_{k=1}^{n} a_k t^k \tag{14}$$

This procedure gives a good fit to the average stress curve for n ranging from 4 to 10; however, when the unit stress is computed from the fitted curve, the existence of local maxima and minima between data points results in wildly oscillating values of unit stress.

An alternative data fitting process was investigated whereby a mathematical expression is assumed for the shape of the unit stress curve based upon the functions that have been used to describe nucleation phenomena in thin films. The number of clusters per unit area above critical size in a growing film after an evaporation time t can be written (Maissel and Glang (Ref. 11)) as

$$N(t) = \frac{1}{D\tau_a}\left(1 - \exp(-I^* D \tau_a t)\right) \tag{15}$$

where D is the surface diffusion coefficient and I* is the nucleation frequency. If we assume that the unit stress in a thin film is proportional to the number of clusters, N(t), then the unit stress function can be written as a function of film thickness x as

$$\sigma(x) = a\,\frac{N(x)}{N^{\infty}} \tag{16}$$

where N^{∞} is the saturation number of nuclei on the substrate. Consequently,

$$\sigma(x) = a\left[1 - \exp(-bx)\right] \tag{17}$$

and the measured stress becomes

$$\langle S(x) \rangle = a - \frac{a[1 - \exp(-bx)]}{bx} \tag{18}$$

The stress behavior of thin films of ThF_4 for large thicknesses also shows a decrease in the equilibrium stress value, which can be thought of as a stress relief effect to the growing number of defects (cracking) as the film thickness

11. L.I. Maissel, R. Glang, Handbook of Thin Film Technology, (McGraw-Hill, New York, 1970) p. 8-15.

increases. Such an effect is modeled by assuming a unit stress function of the form

$$\sigma(t) = a \exp(-bt) \left\{1 - \exp[(b-c)t]\right\} \tag{19}$$

where the term exp(-bt) modifies the stress for large thicknesses.

The average measured stress can be represented by

$$\langle S(t) \rangle = \frac{1}{t} \int_0^t \sigma(t) dr \tag{20}$$

for $t \ll h/2$ and, consequently, the form of this function from equation (19) is

$$\langle S(t) \rangle = \frac{a}{bt} \left[1 - \exp(-bt)\right] - \frac{a}{ct} \left[1 - \exp(-ct)\right] \tag{21}$$

The constants a, b, and c are calculated from a set of average stress data points $\langle S_i(t_i) \rangle$ such that the expression

$$W = \sum_{i=1}^{n_1} \left[\langle S_i(t_i) \rangle - \frac{a}{bt_i} [1-\exp(-bt_i)] + \frac{a}{ct_i} [1-\exp(-ct_i)] \right]^2 \tag{22}$$

is minimized.

The fitted average stress curves are shown in Figures 14 and 15 for thorium fluoride and zinc selenide thin films. These curves are generated from experimental data using the above curve fitting codes, and this procedure enables the data to be reduced to three constants for each type of film. These constants vary with deposition conditions as described in Section 4 but provide a convenient input to a computer model of stress addition in multilayer structures.

3.4 STRESS RELIEF EFFECTS

When a stressed thin film is deposited onto an uncoated disk, the deflection of the disk causes a small amount of stress relief to occur in the film material. Alternatively, if an external force is applied to the center of the plate such that the deflection produced by the film is removed, the film is elongated and the true value of film stress is larger than if the plate were allowed to bend freely. Such stress relief effects also occur when films are added to an existing multilayer structure since a deflection of the plate elongates or contracts the previously deposited film stack.

Fortunately, the magnitude of this effect is very small and such consideration can be neglected for stress addition in multilayer films. The amount of stress relief can be calculated from the unit elongation, ϵ, (Figure 16) which occurs when the curved plate is flattened, i.e.,

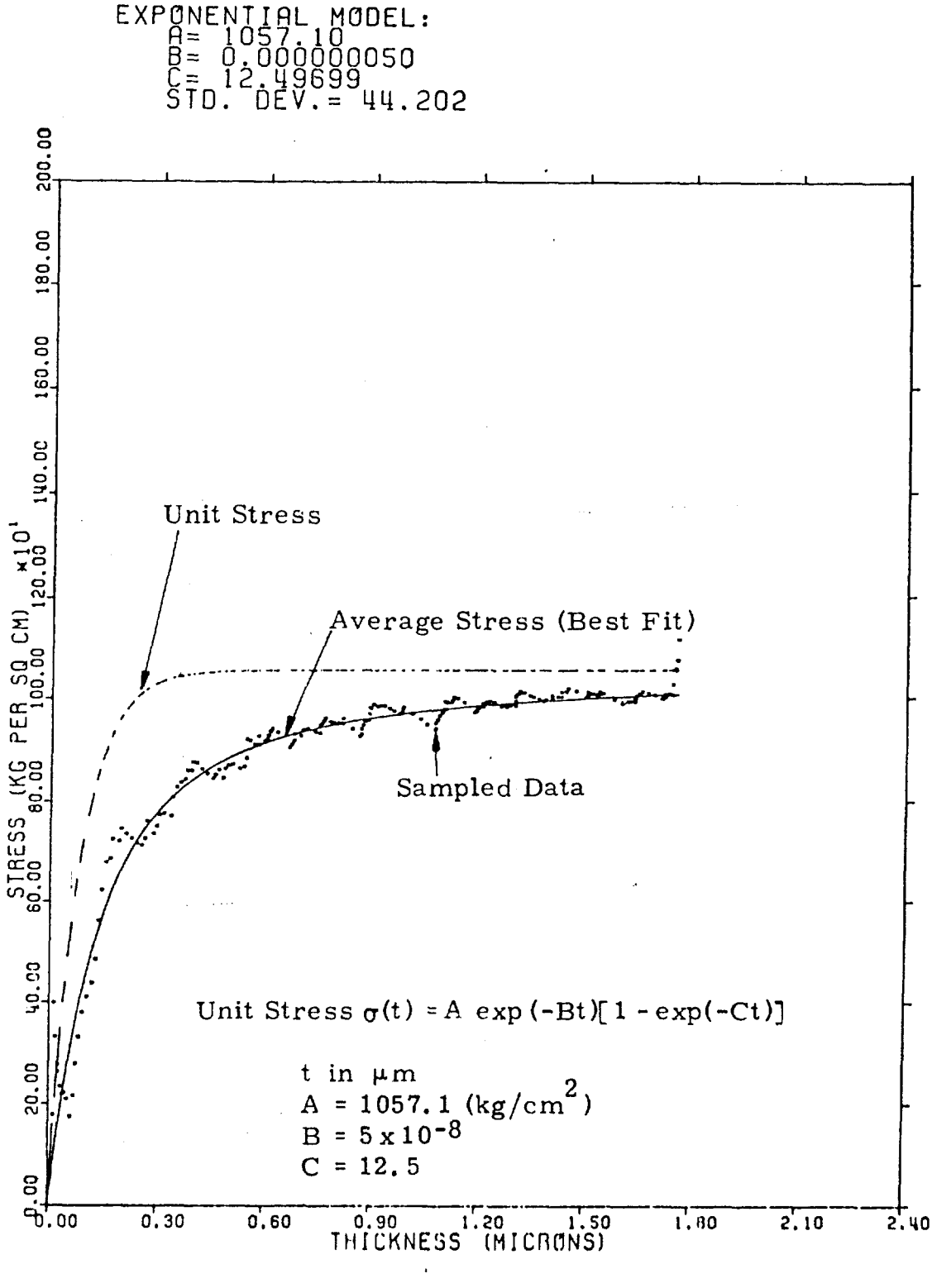

Figure 14. Tensile Stress Produced in Thorium Fluoride Film Material Deposited at 37 Å/s at 200°C. Stress measured from the deflection of 0.5-mm-thick Cer-Vit substrate.

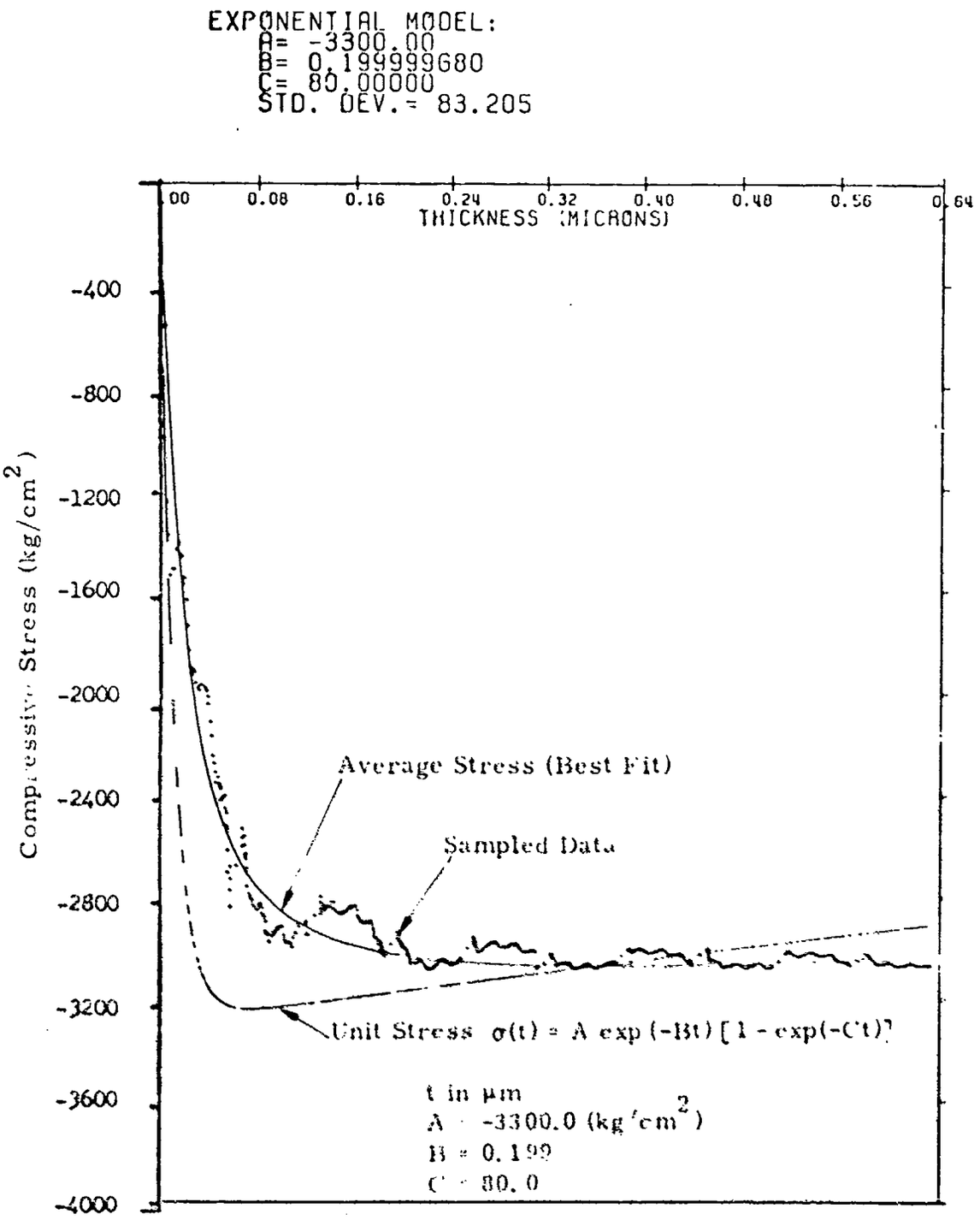

Figure 15. Compressive Stress Produced in Zinc Selenide Thin Film Material Deposited at 4.4 Å/s at 150°C. Stress measured from deflection of 0.25-mm-thick Cer-Vit substrate.

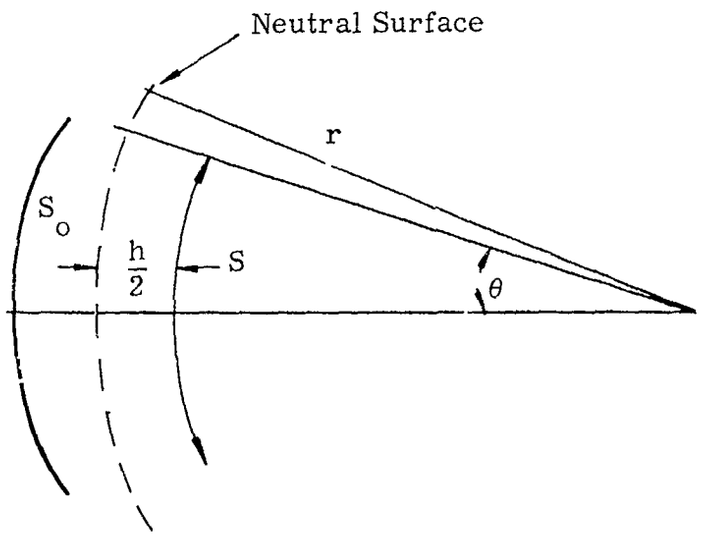

Figure 16. Stress Relief Effects

$$\epsilon = \frac{S_o - S}{S_o} = \frac{r\sigma(r-h/2)\sigma}{(r-h/2)} = \frac{h}{2r-h} \tag{23}$$

Since the radius of the plate, r, is much greater than its thickness, this elongation can be written

$$\epsilon = \frac{h}{2r} = \frac{8\omega h}{2D^2} \tag{24}$$

The initial radius of the plate is related to the plate deflection as given in equation (3) and, consequently, the unit elongation can be written

$$\epsilon = \frac{4\omega h}{D^2} \tag{25}$$

From the definition of Young's modulus for the film material, the induced stress is

$$\sigma = \frac{4E_f \omega h}{D^2} \tag{26}$$

The corrected value of film stress including the stress relief term is thus

$$\langle S \rangle_{total} = \frac{4Es}{3(1-\nu)} \left(\frac{h}{D}^2\right)\left(\frac{\omega}{t}\right) + \frac{4E_f \omega h}{D^2} \tag{27}$$

or, alternatively,

$$\langle S \rangle_{total} = \frac{4Es}{3(1-\nu)} \left(\frac{h}{D}\right)^2 \left(\frac{\omega}{t}\right) \left[1 + \frac{E_f}{E_s} 3(1-\nu) \frac{t}{h}\right] \tag{28}$$

The correction term can be seen to be small, involving the ratio of film thickness to substrate thickness, t/h, assuming that Young's modulus for the film, E_f, and the substrate, E_s, are of comparable size. Consequently, stress relief effects are not included in the data reduction codes for film stress.

The expressions derived thus far relate to deflections of a thin disk caused by the unit stress function and stress relief as the film is being deposited at constant temperature. When the film/substrate combination is cooled in vacuum after deposition, the disk undergoes deflections caused by thermal gradients and differences in expansion coefficient of film and substrate ("bimetallic effects").

3.5 THERMALLY INDUCED STRESS

Since thin films are usually deposited onto hot substrates, the measured values of intrinsic stress pertain to the deposition temperature, and large changes in intrinsic film stress can occur when the coated substrate is cooled after film deposition. During cooling, differential contraction of the film

and substrate due to an expansion coefficient mismatch produces stress changes in the film assuming that no slippage occurs at the film/substrate boundary.

If the film/substrate system undergoes a uniform temperature change ΔT, the unit elongation of film and substrate is ϵ_f and ϵ_s respectively, i.e.,

$$\epsilon_f = \alpha_f \Delta T$$

$$\epsilon_s = \alpha_s \Delta T$$

where α_f and α_s are the thermal coefficients of expansion of the film and substrate material.

Since the film is assumed to adhere to the substrate, it cannot physically elongate more than the substrate elongates; hence, the excess elongation of the film $(\epsilon_f - \epsilon_s)$ can only be prevented by the presence of a compressive stress

$$\sigma_f = E_f(\alpha_f - \alpha_s)\Delta T \tag{29}$$

The values of the expansion coefficient and the Young's modulus for thin films are usually unknown and bulk values are normally utilized for calculation purposes. Since the thermal stress changes can easily exceed the intrinsic stress established during deposition when films are deposited onto high expansion substrates, a method of measuring both quantities was developed using the stress interferometer and is described in Section 5.

3.6 STRESS ADDITION IN MULTILAYER FILMS

Using the expressions derived above, the stress in the i^{th} film of a multilayer stack deposited at a temperature T_i can be written as

$$\sigma_i(t) = A_i \exp(-B_i t)[1 - \exp(-C_i t)] + E_i(\alpha_i - \alpha_s)(T_i - T_o) \tag{30}$$

where T_o is the final temperature of the multilayer stack. The above expression neglects stress relief effects and assumes that the thermally induced stresses are reversible, i.e., no phase changes or film interdiffusion occurs during formation of the multilayer stack. The constants A_i, B_i, C_i are the measured stress coefficients that can depend upon the deposition conditions.

If each film has a thickness t_i, the total bending moment after deposition at some equilibrium temperature T_o is given by

$$M_{STACK} = \int_{h/2}^{h/2 + t_1} [\sigma_1(z) + E_1(\alpha_1 - \alpha_s)(T_1 - T_o)]\, z\,dz$$

$$+ \int_{h/2 + t_1}^{h/2 + t_1 + t_2} [\sigma_2(z) + E_2(\alpha_2 - \alpha_s)(T_2 - T_o)]\, z\,dz + \ldots \tag{31}$$

or in terms of the stress coefficients

$$M_{STACK} = \sum_{i-1}^{m} \int_{h/2 + \sum_{j=1}^{k-1}}^{h/2 + \sum_{j=1}^{k}} \{A_i \exp(-B_i z)[1 - \exp(-C_i z)] + E_i(\alpha_i - \alpha_s)(T_i - T_o)\} \, z\,dz \ldots \quad (32)$$

This expression is a measure of the force acting at the substrate/stack boundary tending to separate the films from the substrate.

The corresponding deflection of the substrate is obtained by substituting the above expression for M into equation (7), i.e.

$$\omega_{TOTAL} = \frac{3}{2}\left(\frac{1-\nu}{E_s}\right)\left(\frac{D^2}{h^3}\right) M_{STACK} \quad (33)$$

If a multilayer stack is formed of materials having opposite stress characteristics it is sometimes possible to arrange for the net bending moment to approach zero after the film substrate combination is cooled to room temperature. Such a film system is usually incorrectly referred to as a zero stress system; however, failure can still occur within the film stack if the sum of the intrinsic and thermal stress is allowed to exceed the breaking stress in any layer. Similarly, the bending moment at intermediate boundaries can exceed the boundary adhesive forces resulting in delamination.

As an aid to describing the stress behavior of thin film systems, a computer code was completed during the program to determine the stress level in the component films of multilayer film stacks. The model utilizes the measured values of the stress coefficients, A_k, B_k, and C_k, together with measured data for thin film expansion coefficients and Young's modulus. This enables stress changes to be determined in each film in the stack at various uniform temperatures. In addition, the total bending moment is calculated for the substrate/film boundary.

The prime motivation for measuring film stresses is to discover methods of changing the intrinsic stress by altering deposition conditions, by utilizing mixtures or by investigating the influence of radiation (UV, visible) upon film formation. The intrinsic stress of ThF_4 films has been found to be relatively insensitive to deposition conditions, whereas ZnSe films show large changes in intrinsic stress with changes in rate and temperature.

SECTION 4

INTRINSIC STRESS MEASUREMENTS

4.1 MATERIAL SELECTION

During the present program two widely utilized infrared materials, thorium tetrafluoride and zinc selenide were investigated in detail and several measurements were made using thallium iodide and cerium fluoride material. Thallium iodide was investigated late in the program because of its increasing importance in the fabrication of IR window antireflection coatings and HEL metal dielectric mirrors (Ref. 12). Cerium fluoride was also characterized to some extent since it is used extensively as a protective overcoat for FLIR windows.

4.2 DEPOSITION CONDITIONS - EXPERIMENTAL

During the present investigation, deposition of ThF_4, ZnSe, TlI, and CeF_3 were carried out using an electron beam source. Changes in vapor incidence angle for a single deposition were obtained by rotating the interferometer to provide incidence angles of 0°, 20°, 30°, and 40° resulting in slightly lower vapor deposition rates and higher spatial nonuniformity in film thickness at higher incidence angles. Changes in deposition rate for the various materials were obtained by altering the input power to the electron beam gun source. During a single evaporation, the entire interferometer system was enclosed in a stainless-steel housing and heated by a large spiral Calrod heater at the top of the chamber. Deposition could be made at temperatures up to 250°C, and the temperature of the substrates was measured using a single thermocouple attached to one of the interferometer housings.

4.3 INTRINSIC STRESS IN THORIUM TETRAFLUORIDE FILMS

Variations in intrinsic stress as a function of film thickness were measured for thorium fluoride films up to 2.0 μm in thickness. Stress measurements were made primarily utilizing Cer-Vit disks since previous measurements (Figure 12) showed that the calculated stress values were relatively independent of the substrate material. Unfortunately, later measurements for ZnSe films showed large stress differences for films deposited onto Cer-Vit and KCl.

4.3.1 Deposition Rate Dependence

The intrinsic stress in ThF_4 materials (Figure 17) shows a small dependence upon deposition rate, low rates (15 - 20 Å/s) producing a tensile stress of +1400 kg/cm^2 while higher rates of 75 Å/s produce lower tensile stresses of +1100 kg/cm^2.

12. M.C. Ohmer, Private Communication, Air Force Materials Laboratory, Wright-Patterson AFB, Ohio.

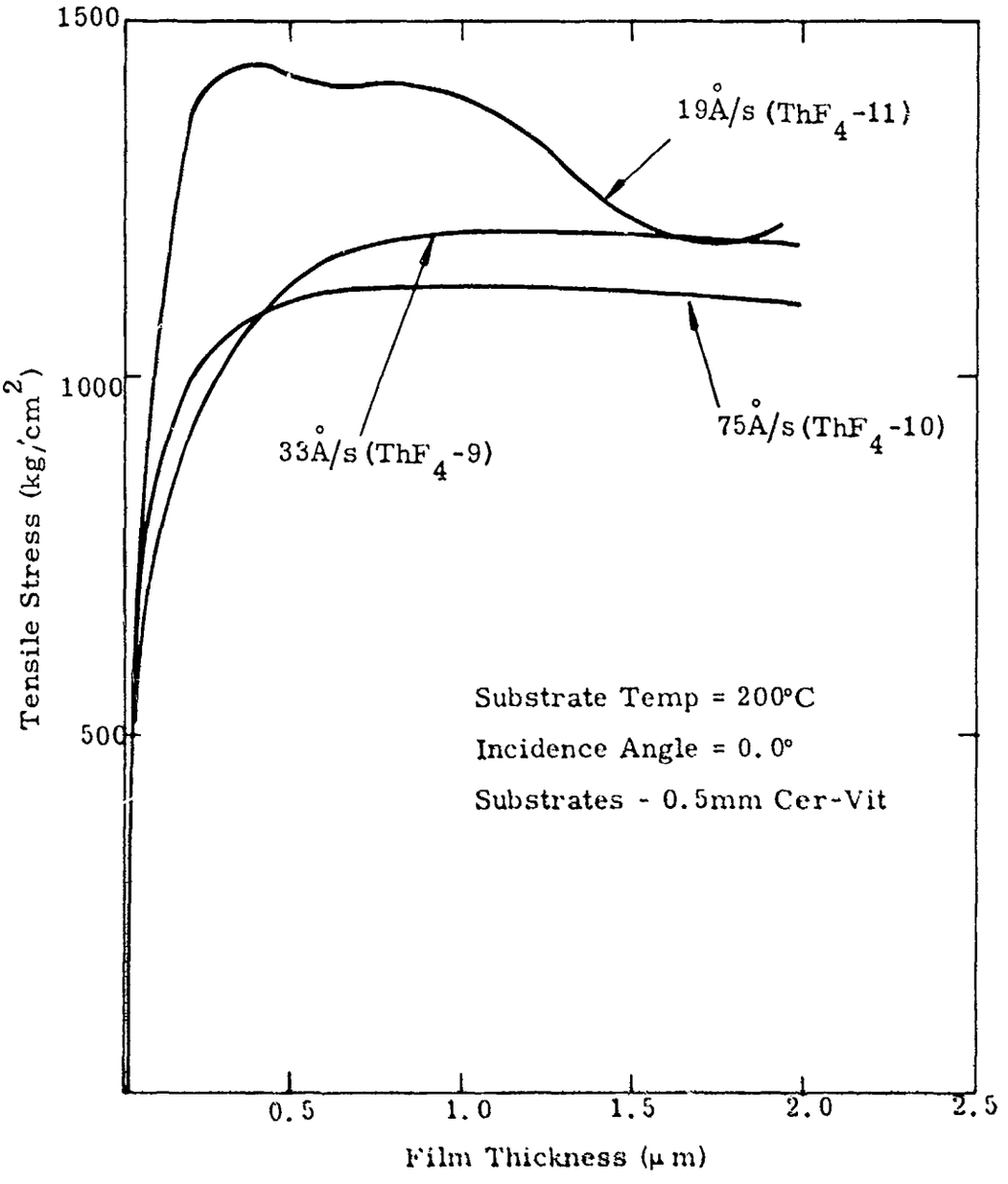

Figure 17. Dependence of Intrinsic Stress in ThF_4 Films on Thickness. Stress Measured using 0.5 mm Thick Cer-Vit Disks and Electron Beam Gun Deposition at 200°C.

4.3.2 Substrate Temperature Dependence

Variation in substrate temperature between 100°C and 200°C has little effect upon the intrinsic stress at large thicknesses (Figure 18); however, the quasi-equilibrium value is reached for smaller film thicknesses as the substrate temperature is reduced. A previous measurement of $ThOF_2$ deposition at ambient temperature is included in Figure 18 for comparison.

4.3.3 Dependence of Stress Upon Incidence Angle

Figures 19 and 20 show the variation of stress with incidence angle for two different substrate temperatures. At extreme angles (>40°) the stress levels at large thicknesses exhibit a large decrease for the 150°C deposition, whereas deposition at 200°C produces a well-defined minimum stress level between 1.0 and 1.7 μm mechanical thickness. These changes are relatively unimportant since large vapor incidence angles are avoided if possible in most thin-film depositions.

4.3.4 Nonuniform Stress Distribution in ThF_4 Films

The experimentally measured values of intrinsic stress for ThF_4 show little dependence upon incidence angle or substrate temperature and a mild dependence upon deposition rate. All measurements indicate a variation of unit stress with thickness with a maximum stress occurring at a thickness in the 0.25-μm range. The effect of such a stress variation of unit stress with thickness can be seen when cracked films of ThF_4 are viewed through an interference microscope as shown in Figure 21(a). The cracked film was produced by depositing ThF_4 ($\lambda/4$ at 10.6 μm) onto KCl at 100°C and heating to 250°C in vacuum after deposition. The flakes show circular fringes indicative of a slow variation of unit stress with film thickness.

4.3.5 Stress Coefficients for ThF_4 Films

Stress coefficients were measured for a ThF_4 film $\lambda/2$ at 10.0 μm using best fit routines. Thin film was deposited at 200°C. The unit stress being given by three coefficients:

$$A = 1057 \text{ kg/cm}^2$$
$$B = 5 \times 10^{-8}$$
$$C = 12.5$$

4.4 INTRINSIC STRESS IN ZINC SELENIDE FILMS

Intrinsic stress measurements for ZnSe films show a much larger dependence upon deposition conditions than do measurements obtained for ThF_4 films. Measurements were made for films up to 2.4 μm thick ($\sim\lambda/2$ at 10.0 μm) at deposition temperatures of 200°C, 150°C, and 200°C for three rates of deposition, the highest and lowest deposition rates being limited by the vapor source characteristics and the chamber configuration.

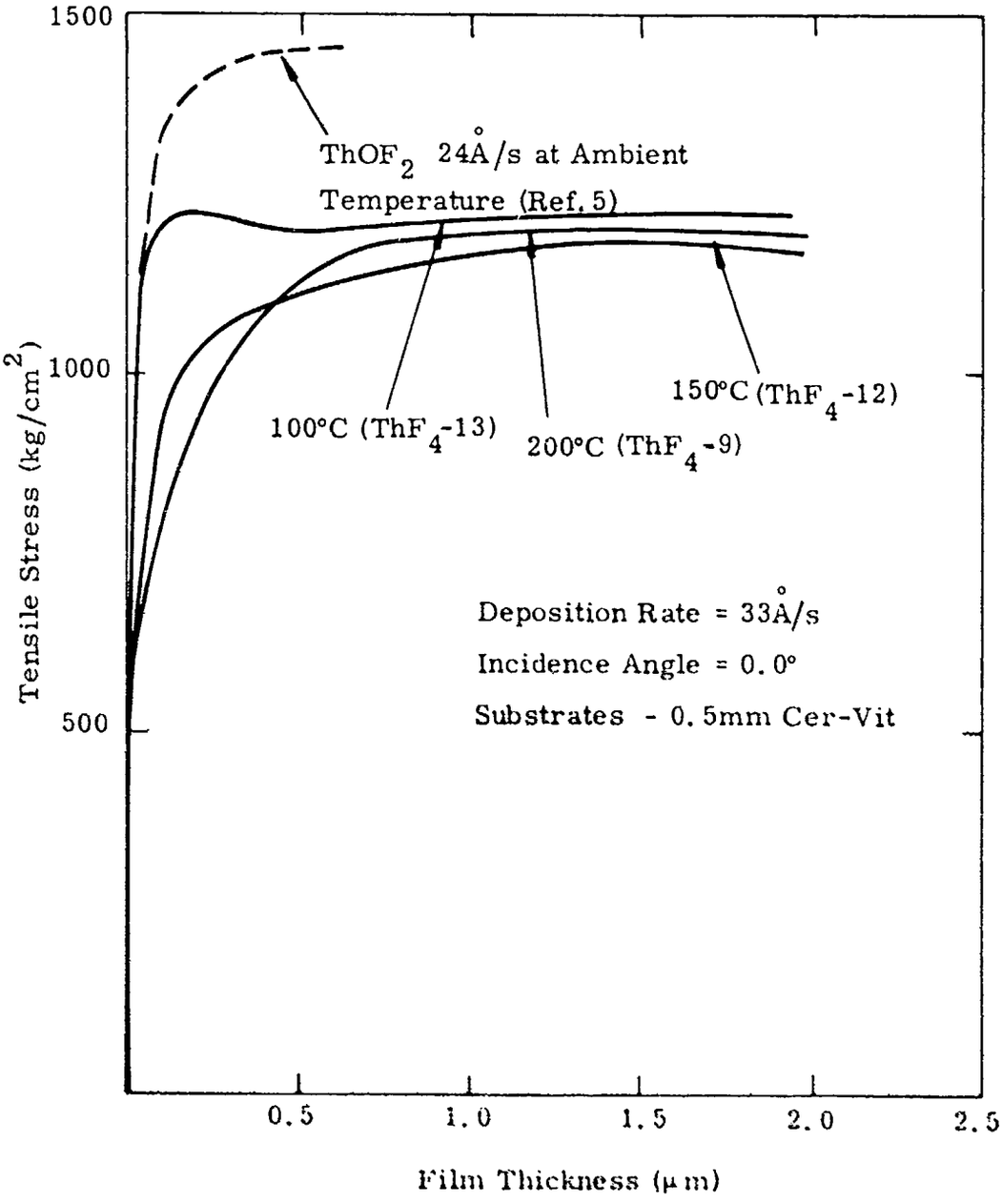

Figure 18. Intrinsic Stress Dependence of ThF_4 Films on Substrate Temperature. Stress measured using 0.5-mm Cer-Vit disks and electron beam deposition at ~33Å/s.

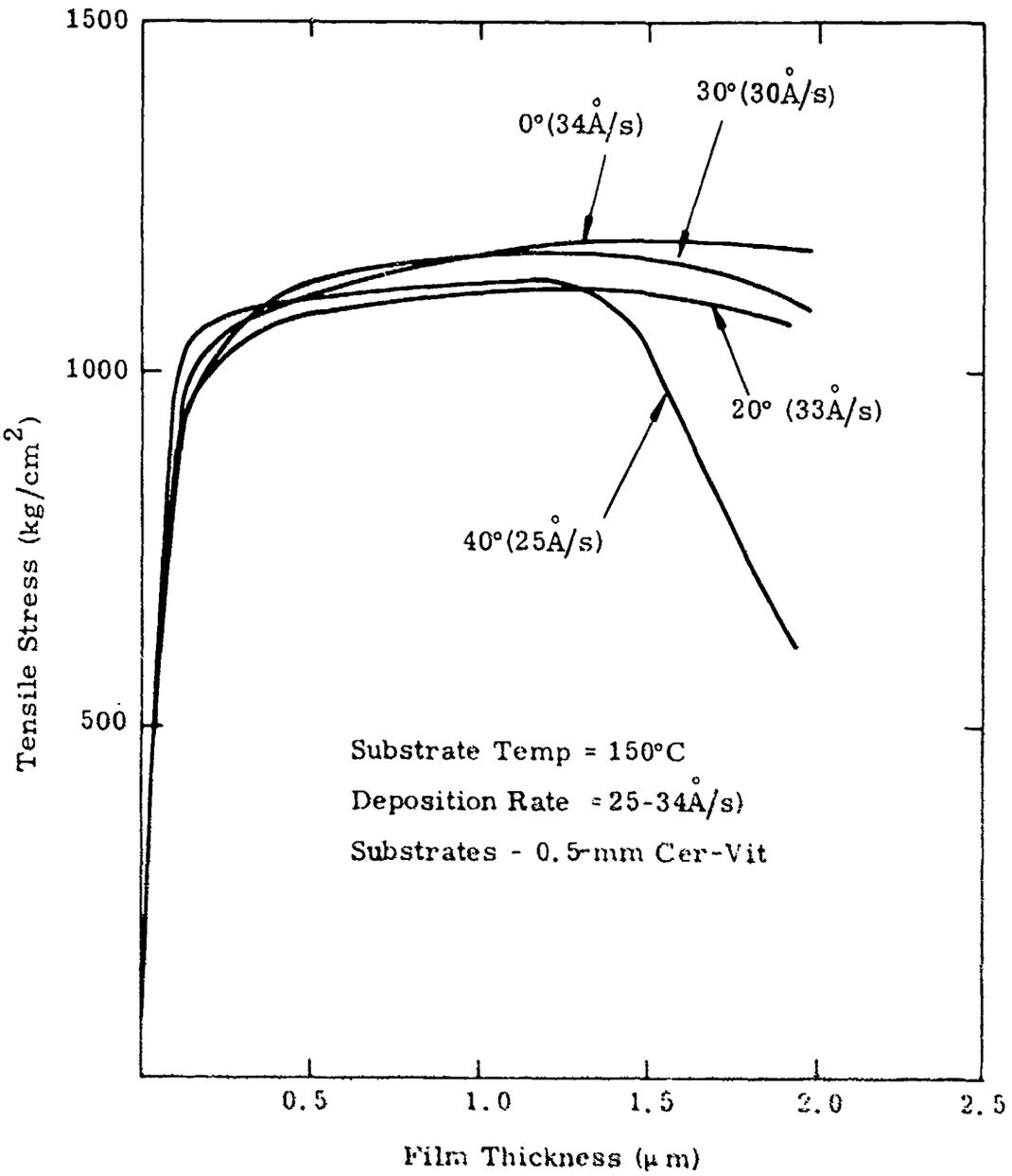

Figure 19. Variation of Intrinsic Stress with Incidence Angle for ThF_4 Films Deposited at 150°C. Stress measured using 0.5-mm Cer-Vit disks; electron beam gun deposition ~ 34Å/s.

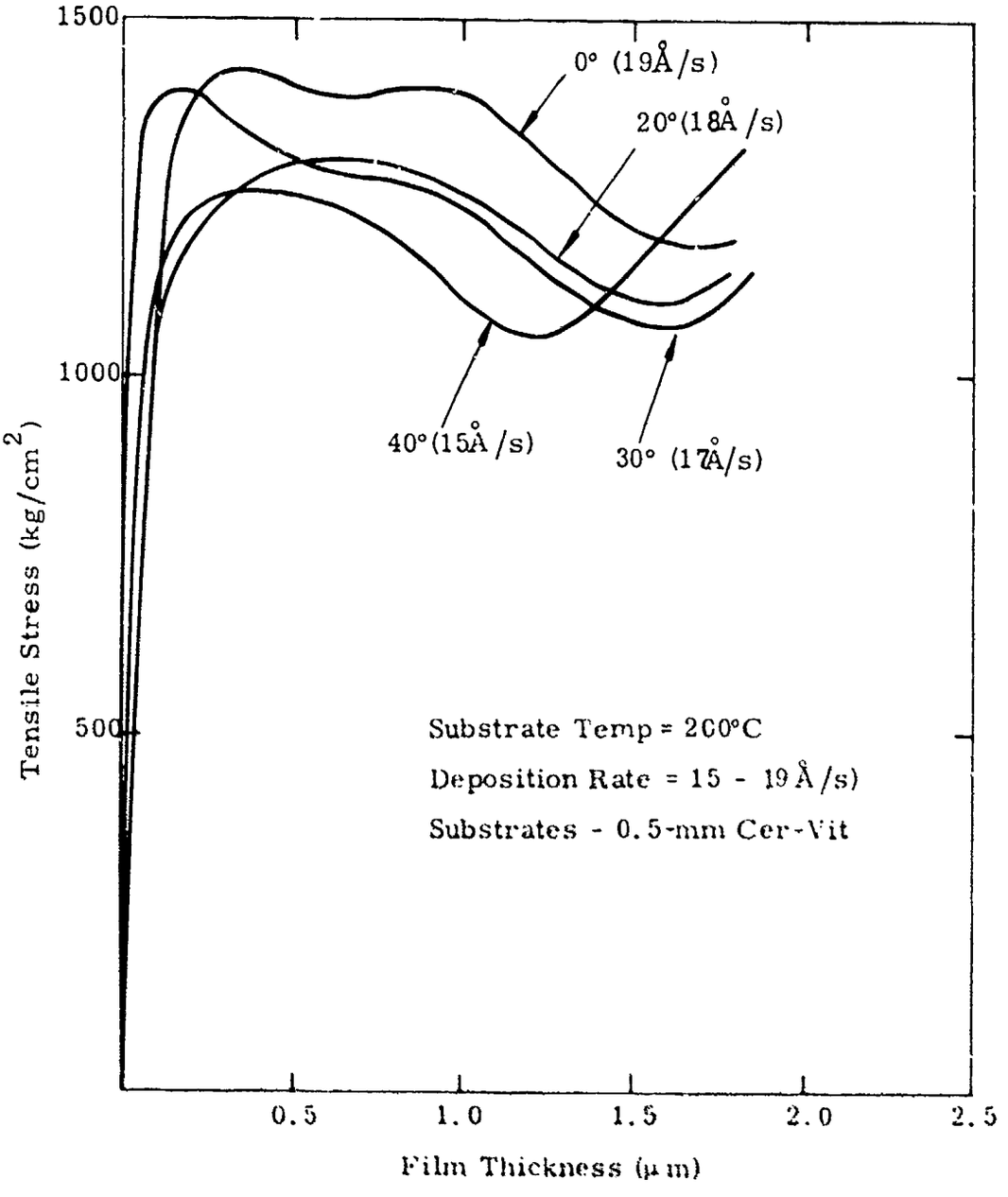

Figure 20. Variation of Intrinsic Stress with Incidence Angle for ThF_4 Films Deposited at 200°C. Stress measured using 0.5-mm Cer-Vit disks and electron beam gun deposition at 34 Å/s.

(a) Cracked ThF_4 Film on KCl. Fringe Curvature Indicates Intrinsic Stress Variation With Film Thickness

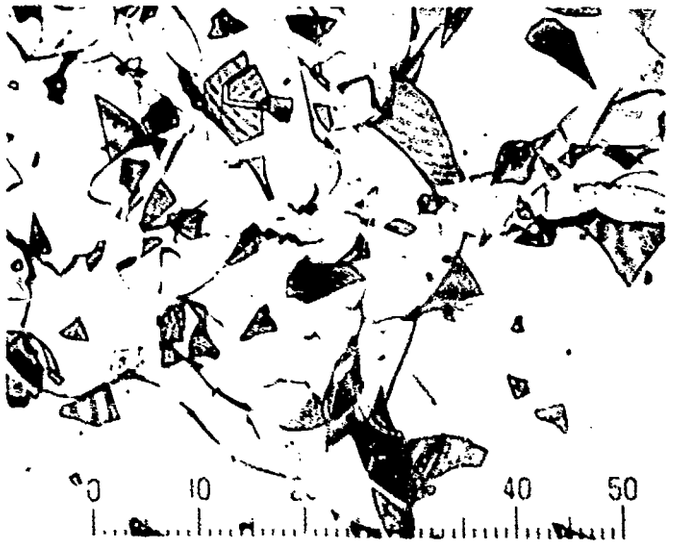

(b) Cracked ZnSe Film on KCl. Pattern Shows Predominantly Straight Fringes

Figure 21. Fringe Patterns Produced for Cracked Films Deposited onto KCl

The dependence of intrinsic stress for ZnSe is shown in Figures 22, 23, and 24 and indicates that a large amount of stress control can be obtained by varying the source rate. Low deposition rates of 2 to 4 Å/s produce high compressive stresses in the 2800 to 3200 kg/cm range whereas the highest rates of deposition, 20 to 25 Å/s, produce compressive stresses in the 1100 to 1800 kg/cm^2 range.

This reduction in stress is offset to some extent by an increase in intrinsic stress with substrate temperature.

4.4.1 Stress Coefficients for ZnSe Films

Stress coefficients for various rates and temperatures for zinc selenide films ($\lambda/2$ at 10.6 μm) are given in Table 2.

TABLE 2. STRESS COEFFICIENTS FOR ZnSe FILMS

Temperature (°C)	Rate (Å/s)	A	B	C
100	2.6	-5150	2.05	25.0
100	18	-2100	0.95	56.0
100	18	-1866	0.58	60.0
150	4.4	-3300	0.20	80.0
150	20.0	-2200	0.94	68.2
150	24.0	-2384	0.9	74.3
200	3.0	-4640	1×10^{-9}	9.0
200	19.0	-3800	0.01	21.5
200	24.0	-3020	0.44	82.5

4.4.2 Nonuniform Stress Distribution in ZnSe Films

In general, the rate of rise of stress with increased film thickness for ZnSe films is much faster than for ThF_4 films and is followed by a steady decrease with an increase in thickness. Observation of flakes of zinc selenide films (Figure 21(b)) tend to confirm this thickness-dependent stress behavior showing predominantly straight line fringes for most of the cracked samples observed.

4.5 INTRINSIC STRESS IN THALLIUM IODIDE AND CERIUM FLUORIDE FILMS

Deposition of thallium iodide films ($\lambda/2$ at 10.6 μm) at rates of 4 Å/s and 20 Å/s shows that the stress in this material is extremely low. Using the thinnest fused silica slides available (0.18 mm thick x 19 mm diameter) the maximum fringe count obtained corresponded to a stress of less than 50 kg/cm^2. This compares with previous values measured for thinner films by Ennos (Ref. 5) of 200 kg/cm^2.

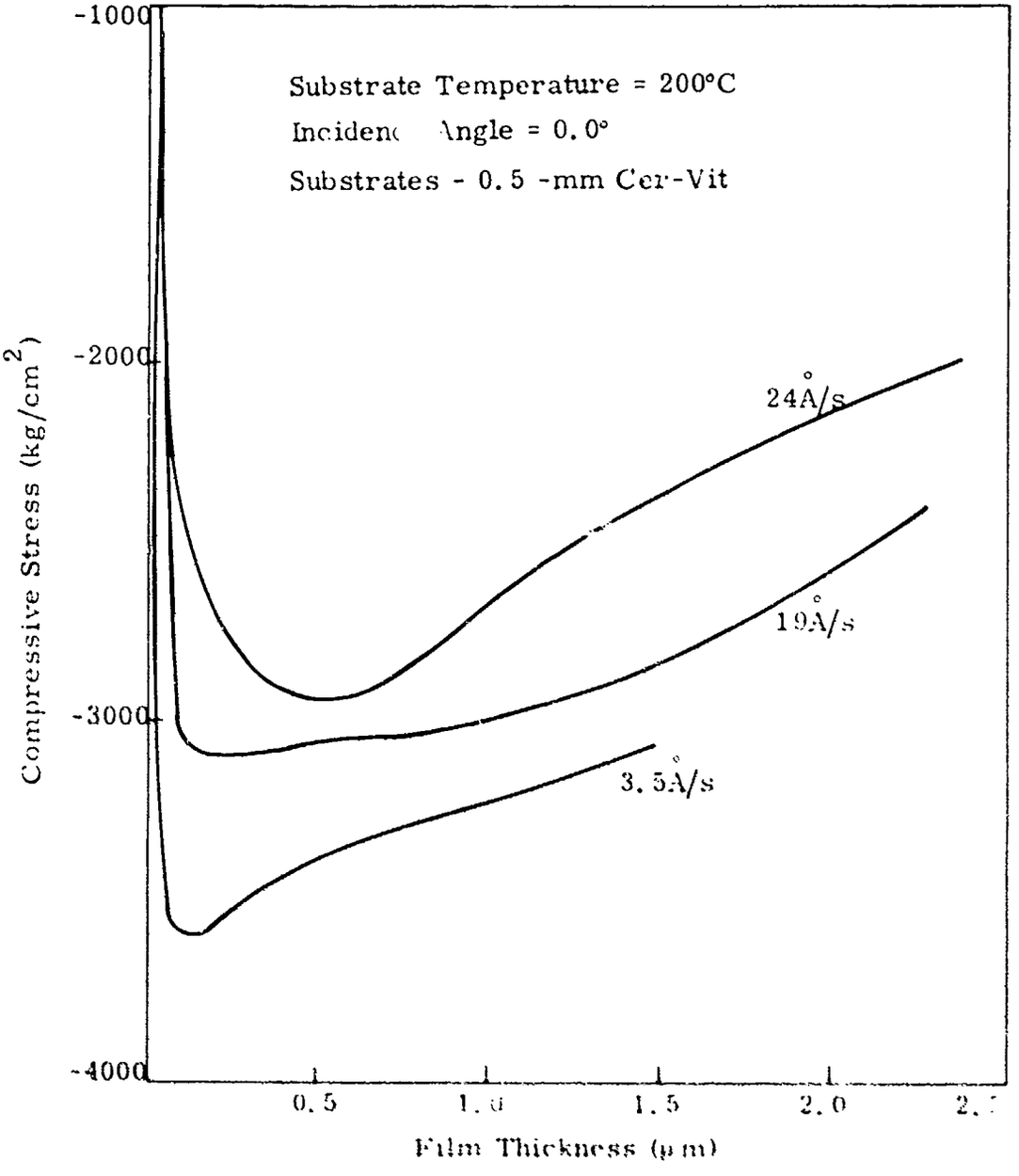

Figure 22. Variation of Intrinsic Stress in Zinc Selenide with Deposition Rate (Source Controlled). Stress measurements made using 0.25-mm Cer-Vit disks at a substrate temperature of 200°C.

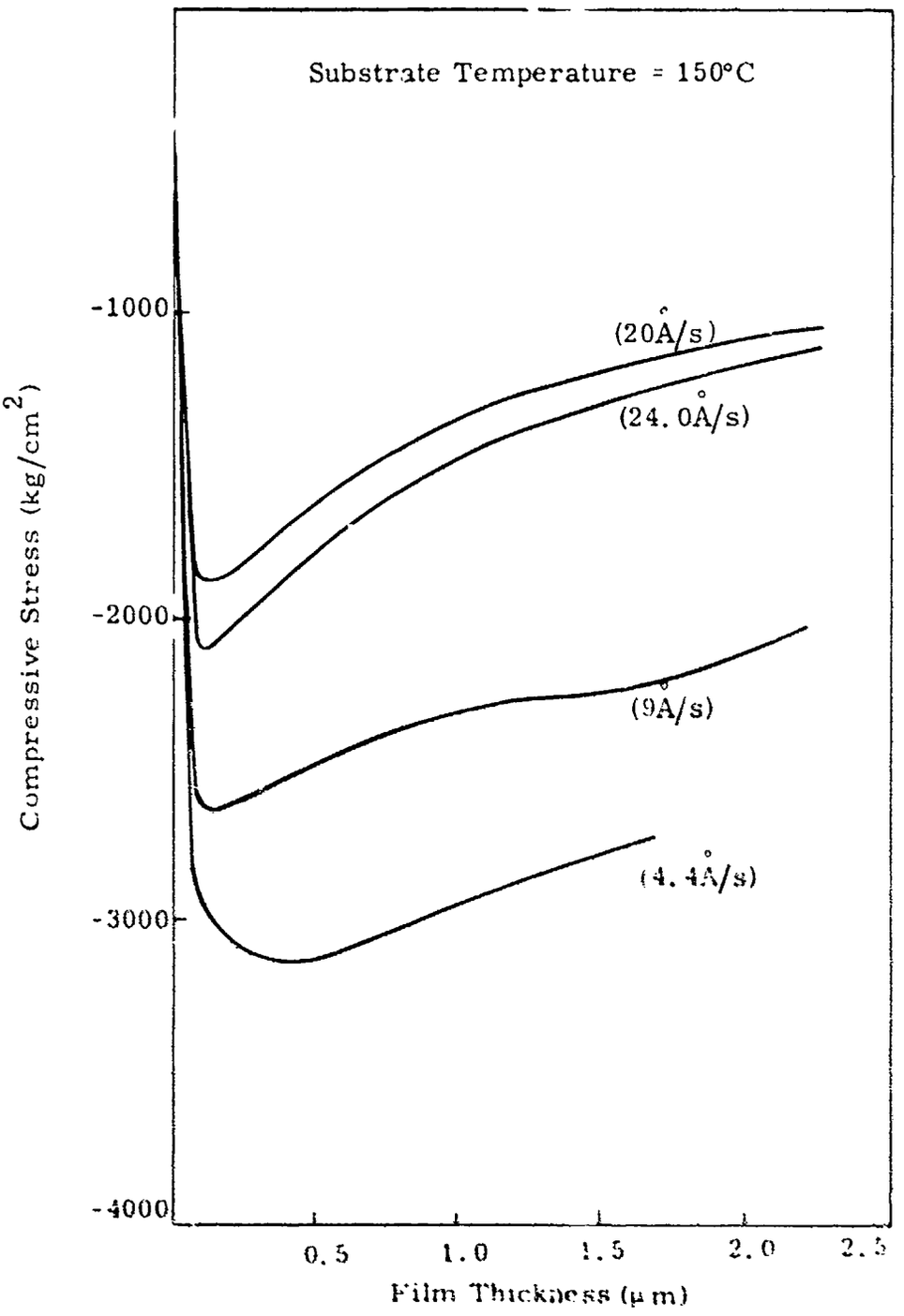

Figure 23. Variation of Intrinsic Stress in Zinc Selenide Films with Deposition Rate (Source Controlled). Stress measurements made using 0.25-mm Cer-Vit Disks at a temperature of 150°C.

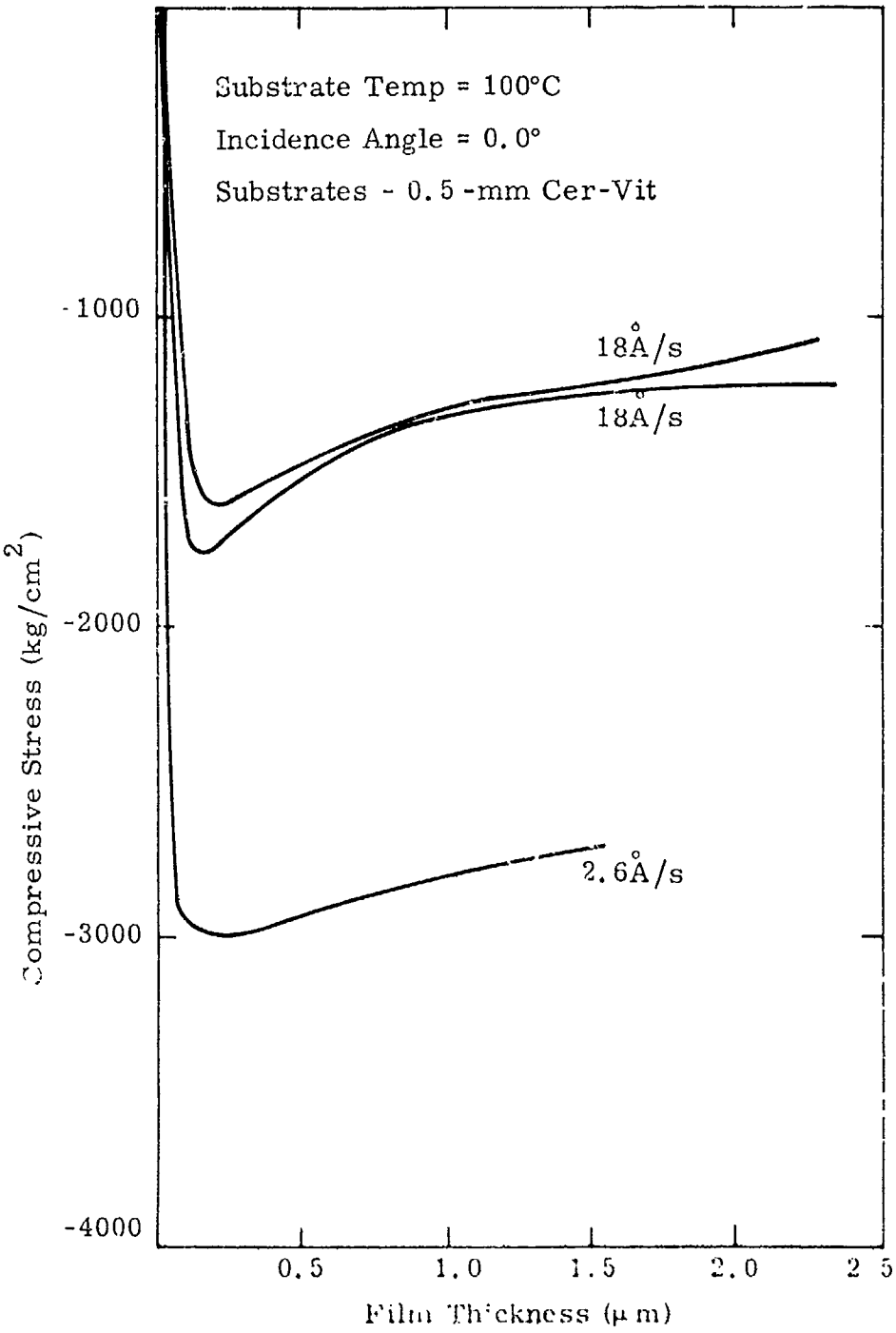

Figure 24. Variation of Intrinsic Stress in Zinc Selenide Films with Deposition Rate (Source Controlled). Stress Measurements made using 0.25-mm Cer-Vit Disks at a Substrate Temperature of 100°C.

Cerium fluoride films were also evaluated and show highly tensile behavior together with a small disruptive film thickness. The variation of tensile stress for this material is given in Figure 25.

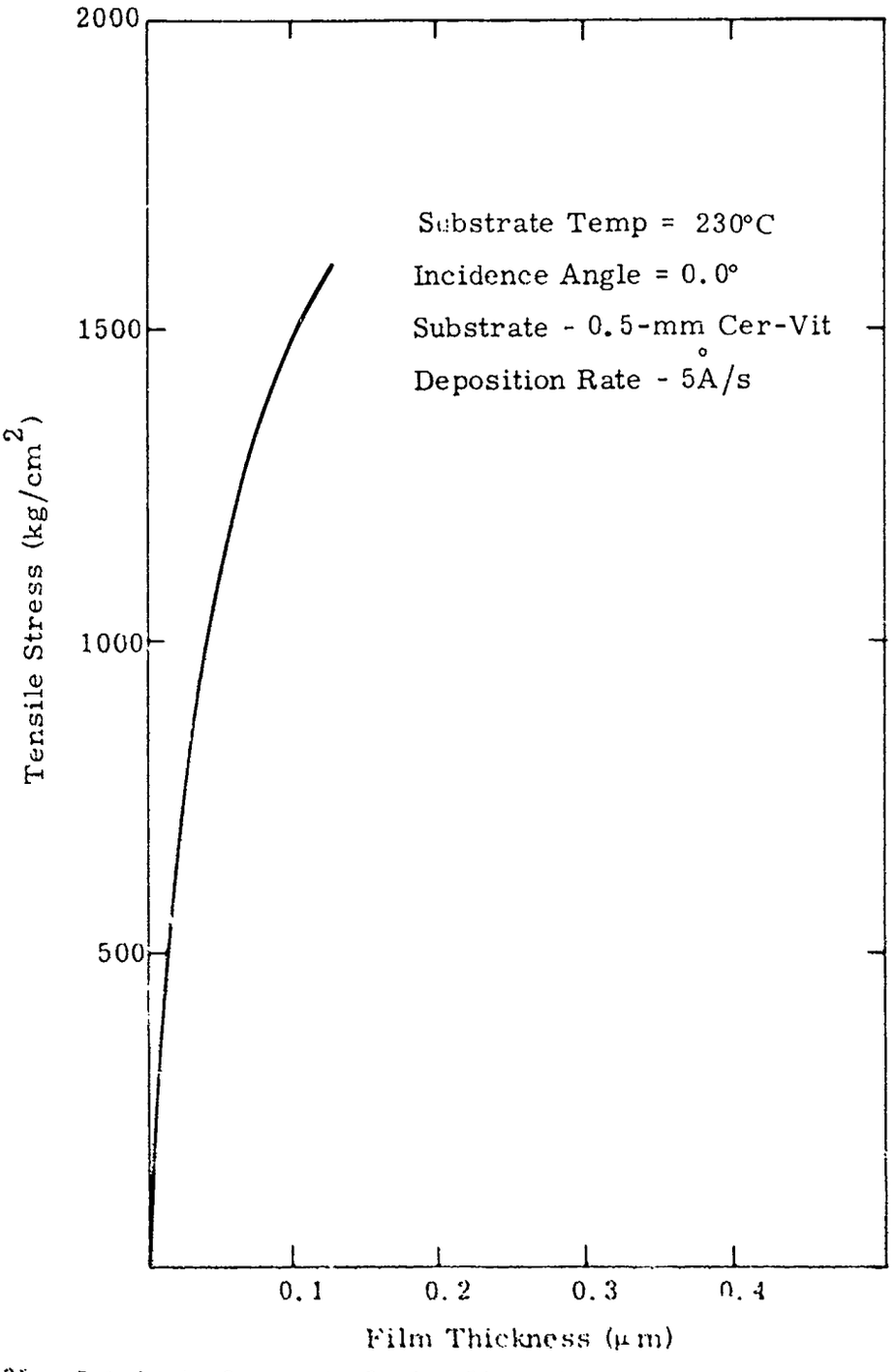

Figure 25. Intrinsic Stress in Cerium Fluoride Film Deposited at 230°C by Electron Beam Gun. Stress Measured using Cer-Vit 0.5 mm Thick.

SECTION 5

MECHANICAL PROPERTY MEASUREMENTS

5.1 EXPANSION COEFFICIENT AND YOUNG'S MODULUS DETERMINATION FOR THIN-FILM MATERIALS

Experimental values of the thermal expansion coefficient (α_f) and Young's modulus (E_f) for a thin film can be obtained using the four-channel interferometer system by observing the total deflection caused by thermally induced stress. Figure 26 shows the output from two interferometer channels during deposition of a film of ThF_4 ($\lambda/4$ at 10.6 μm) and during subsequent cooldown. This film is deposited onto Cer-Vit and KCl disks and the thermally induced stress contribution is sufficient to produce a large tensile stress (+3400 kg/cm^2) for ThF_4 on Cer-Vit and a large compressive stress (-1400 kg/cm^2) for ThF_4 deposited onto KCl. When zinc selenide films are deposited onto KCl in this manner the large initial intrinsic stress -(1500 - 3000) kg/cm^2 together with a thermally induced stress of ~2400 kg/cm^2 is usually sufficient to crack the films by compressive film failure at the -4000 to -5000 kg/cm^2 stress level.

Initial experiments using uncoated disks of various materials showed that substantial fringe changes occurred upon heating and cooling presumably due to temperature gradients (radial and front to back) existing in the flexible disks. Experimental measurements were therefore made using all four interferometers and coated and uncoated disks of each substrate maerial. Fringe changes were utilized on cooldown since this results in a much lower cooling rate than during the heatup cycle.

The values of expansion coefficient and Young's modulus can be obtained from the expressions for the thermally induced deflection of a thin disk, i.e.,

$$w = \frac{3(1-\nu_s)t}{4E_s}\left(\frac{D^2}{h}\right) E_f(\alpha_f - \alpha_s)\ (T_i - T_o)$$

where $(T_i - T_o)$ is the total temperature change, α_s, ν_s, and E_s being the expansion coefficient, Poisson's ratio, and Young's modulus, respectively, of the substrate.

For two different substrate materials each coated with a film of thickness t the thermally induced deflections are

$$w_1 = \frac{3(1-\nu_1)t}{4E_1}\left(\frac{D_1^2}{h_1}\right) E_f(\alpha_f - \alpha_1)\ (T - T_o)$$

$$w_2 = \frac{3(1-\nu_2)t}{4E_2}\left(\frac{D_2^2}{h_2}\right) E_f(\alpha_f - \alpha_2)(T - T_o)$$

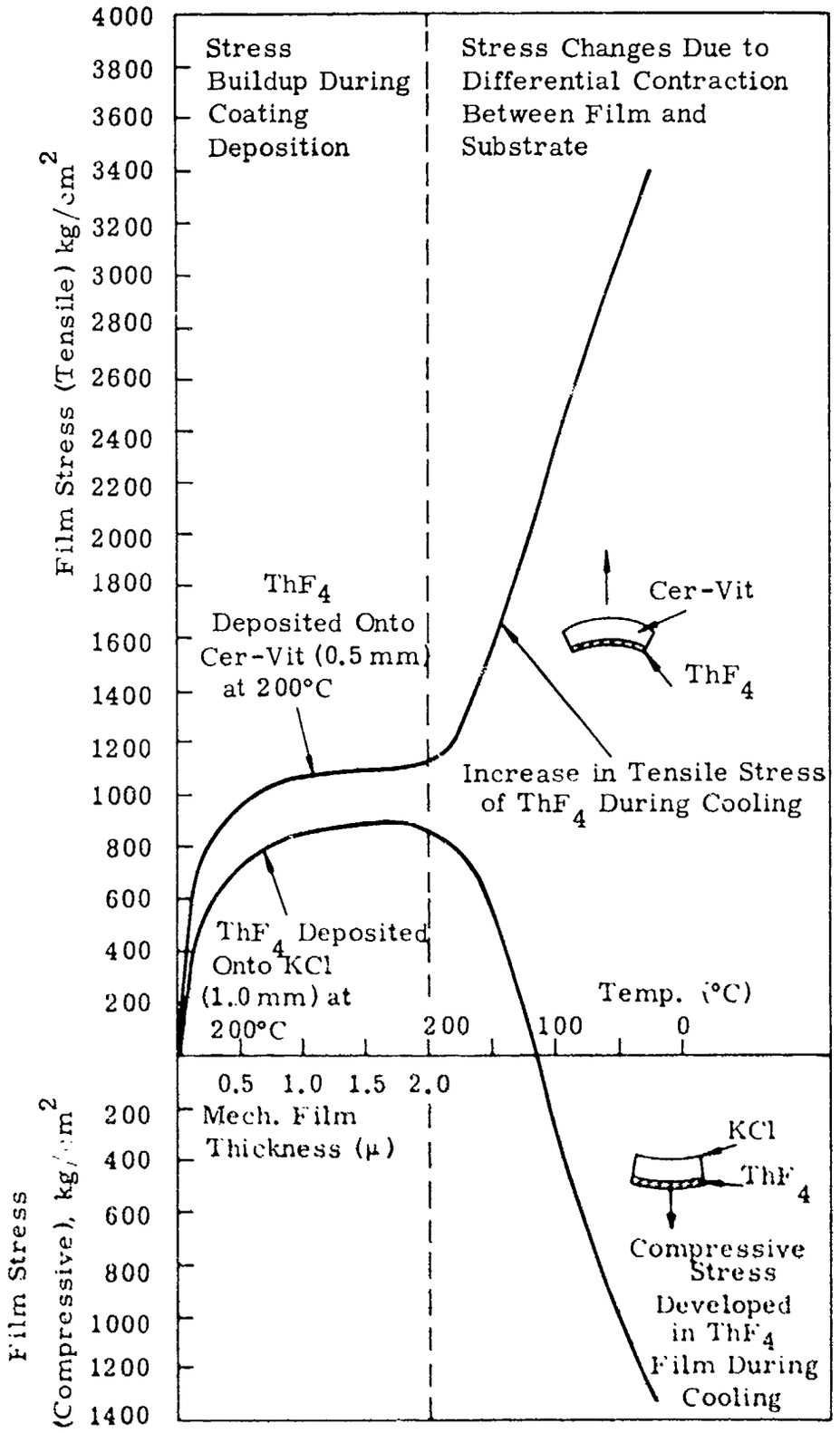

Figure 26. Intrinsic and Thermally Induced Stresses in ThF4 Films Deposited Onto Cer-Vit and KCl Substrates at 200°C

Consequently, the values of the film constants α_f and E_f are given by

$$\alpha_f = \frac{\alpha_2 \omega_1 \Lambda_2 - \alpha_1 \omega_2 \Lambda_1}{\omega_1 \Lambda_2 - \omega_2 \Lambda_1}$$

$$E_f = \frac{\omega_2}{\Lambda_2 (\alpha_f - \alpha_2)\, t\, (T - T_o)}$$

where

$$\Lambda_1 = \frac{3(1 - \nu_1)}{4E_1} \left(\frac{D_1^2}{h_1}\right) \quad \text{and} \quad \Lambda_2 = \frac{3(1 - \nu_2)}{4E_2} \left(\frac{D_2^2}{h_2}\right)$$

characterize the substrate properties.

In all experimental determinations the deflections ω_1 and ω_2 correspond to the differences in deflection between the coated and uncoated substrates, i.e.,

$$\omega_1 = (\omega_1)_c - (\omega_1)_{uc}$$

$$\omega_2 = (\omega_2)_c - (\omega_2)_{uc}$$

5.2 EXPERIMENTAL RESULTS

The typical changes that occur during heating, cooling, and reheating of coated and uncoated disks of different materials are shown in Figure 27. Here, disks of Cer-Vit and KCl are coated with ThF_4 material, and the fringe changes as a function of temperature are used to compute the expansion coefficient and Young's modulus of the thin-film material as shown above.

Measurements were made of thin films of ThF_4, ZnSe, TlI in this manner and the results are summarized in Table 3.

Emphasis was placed on obtaining values of α_f for thorium tetrafluoride since measurements of this material in single crystal form by Van Uitert (Ref. 13) show that the expansion coefficient is small and negative in the region from 0 to 200°C. The experimental values for thin films consistently showed a large positive value both for measurements made during cooldown and immediately after the film was deposited and during subsequent reheating cycles. Different pairs of substrates (KCl + Cer-Vit and KCl + ZnSe) were also used for these experiments and gave similar results.

The expansion coefficient of thallium iodide material was so closely matched to that of the KCl substrate that no discernible difference in the fringe changes could be seen for the coated and uncoated substrates.

13. L. Van Uitert, et al., Mat. Res. Bull. 11, 669 (1976).

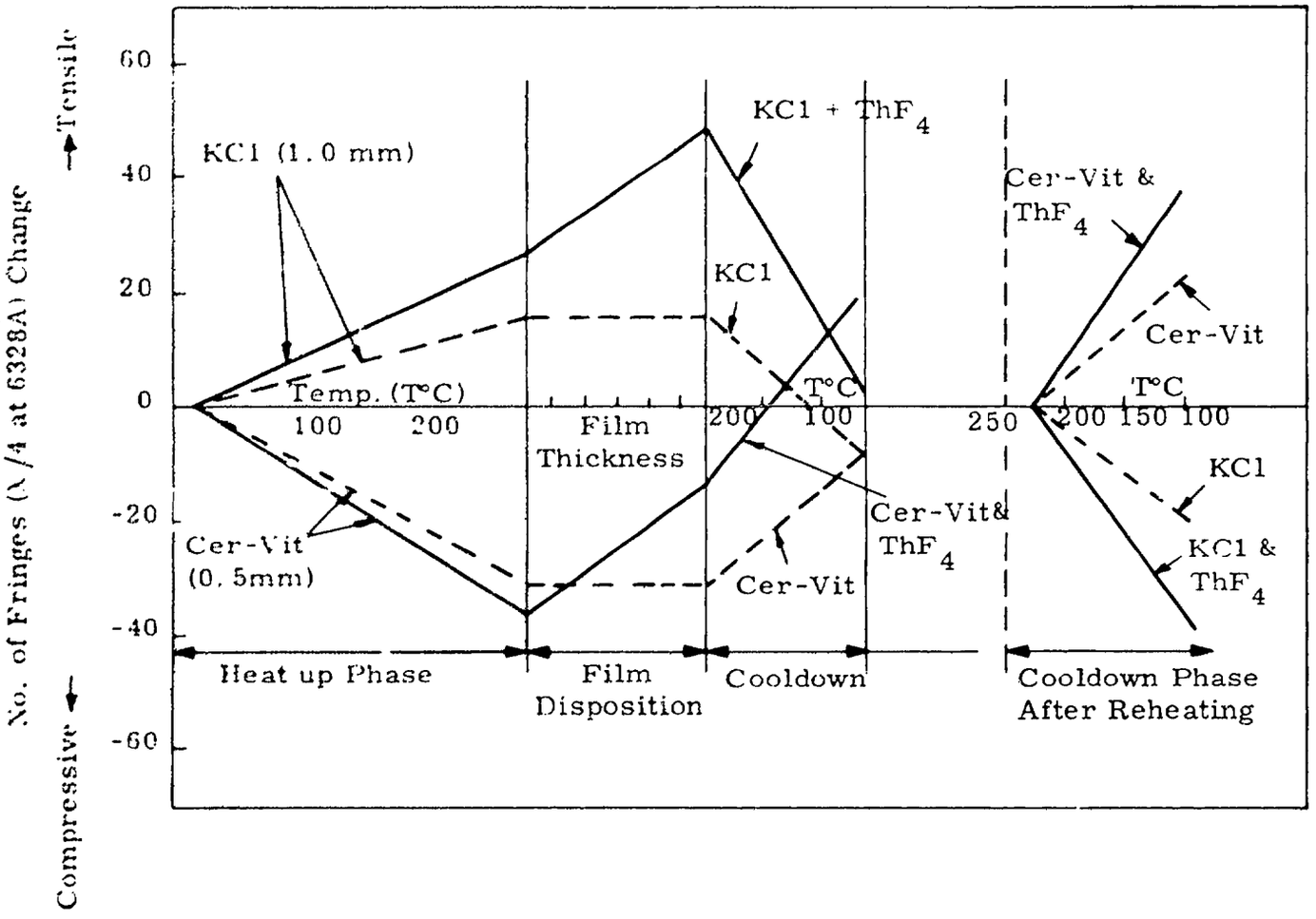

Figure 27. Fringe Changes for λ/4 Film of ThF_4 Deposited onto KCl and Cer-Vit during Heating, Deposition, and Heat Cycling

TABLE 3. EXPANSION COEFFICIENT AND YOUNG'S MODULUS DETERMINATION

Substrates Utilized	Film Material	Film Expansion Coefficient (α_f)	Young's Modulus (Ef)
KCl, Cer-Vit	ThF_4	13.3×10^{-6}/°C	4.3×10^5 kg/cm^2
KCl, Cer-Vit	ThF_4	11.1×10^{-6}/°C	3.9×10^5 kg/cm^2
KCl, ZnSe	ThF_4	18.1×10^{-6}/°C	6.8×10^5 kg/cm^2
KCl, ZnSe	ThF_4	15.1×10^{-6}/°C	4.3×10^5 kg/cm^2
KCl, ZnSe	TlI	36.0×10^{-6}/°C	2.3×10^5 kg/cm^2
KCl, Cer-Vit	ZnSe	8.1×10^{-6}/°C	4.2×10^5 kg/cm^2

SECTION 6

SUMMARY AND CONCLUSIONS

The work performed during the present program has resulted in

- Fabrication of a four-channel stress interferometer system that is capable of measuring stress levels in films as they are being deposited in the form of single layers or as part of multilayer films.
- A new experimental technique has been established whereby the thermal expansion coefficient and Young's modulus of thin-film materials can be measured interferometrically.
- A computer code has been developed that utilizes the experimentally measured values of intrinsic stress, expansion coefficient, and Young's modulus to model the stress levels in multilayer coatings when subjected to a changing uniform temperature environment.

REFERENCES

1. R.W. Hoffman, Physics of Thin Films, Vol. 3, p. 211 (1966).

2. R.W. Hoffman, Thin Solid Films, Vol. 34, p. 185 (1976).

3. K. Kinosita, Thin Solid Films, Vol. 17, p. 17 (1972).

4. R.S. Carpenter and D.S. Campbell, J. Matl. Sci., Vol. 2, p. 173 (1967).

5. A.E. Ennos, Appl. Opt., Vol. 5, No. 1, p. 51 (1966).

6. J.S. Halliday, T.B. Rymer, and K.H.R. Wright, Proc. Roy. Soc. (London) A225, p. 548 (1954).

7. A. Kinabara, H. Harabi, J. Appl. Phys. (Japan), Vol. 4, p. 243 (1965).

8. K. Roll and H. Hoffman, Rev. Sci. Inst., Vol. 47, No. 9 (1976).

9. L.S. Combes, S.S. Ballard, and K.A. McCarthy, J. Opt. Soc. Am., Vol. 41, p. 215 (1951).

10. S. Timoshenko, Theory of Plates and Shells, 2nd ed. (McGraw-Hill, New York, 1959) p. 43.

11. L.I. Maissel and R. Clang, Handbook of Thin Film Technology, (McGraw-Hill, New York, 1970), p. 8 - 15.

12. M.C. Ohmer, Private Communication, Air Force Materials Laboratory, Wright-Patterson AFB, Ohio.

13. L. Van Uitert, et al., Matl. Res. Bull, Vol. 11, p. 669 (1976).

APPENDIX A

WAVEFORM ASYMMETRY FOR CAT'S-EYE INTERFEROMETER

The waveform asymmetry obtained from a cat's-eye interferometer can be modeled by using the field equations for Gaussian beams given by Kogelnik and Li (Ref. A-1). Figure A-1 shows the multiple reflections arising from apparent beam waists at distances 2δ, 4δ, 6δ, etc., due to a mirror separation δ. These spherical waves having Gaussian amplitude profiles are all described at a point z along the axis by a radial electric field given by

$$E(r,z) = \frac{1}{\omega}\left(\frac{2P}{\pi}\right) \exp\left[-j(kz - \phi)\right] \exp\left[-r^2\left(\frac{1}{\omega^2} + \frac{jk}{2R}\right)\right] \tag{A-1}$$

where

$$R(z) = 2\left[1 + \left(\frac{\pi \omega_1^2}{\lambda^2}\right)^2\right] \tag{A-2}$$

$$\omega^2(z) = \omega_1^2\left[1 + \left(\frac{\lambda^2}{\pi \omega_1^2}\right)\right]^2 \tag{A-3}$$

$$\phi(z) = \tan^{-1}\left(\frac{\lambda z}{\pi \omega_1^2}\right) \tag{A-4}$$

Here ω_0 is the beam waist at the first mirror and z is the distance to the summation point of the apparent beam waists.

The radial intensity ω_1, ω_2, ω_3, etc., at a point z_1 is therefore obtained as a coherent summation of all the spherical waves reflected by the mirror surfaces whose individual amplitude reflectivities are given by R_1 and R_2. The radial intensity can be written as

$$I(r,z) = \frac{2P}{\pi} \sum_{i=1}^{\infty} \frac{P_i}{\omega_1} \exp\left[-j(kz_i - \phi_2) - \frac{r^2}{\omega_i^2} + \frac{jkr^2}{2R_i}\right] \sum_{i=1}^{\infty} \frac{P_i}{\omega_i} \exp\left[+j(kz_i - \phi_2) - \frac{r^2}{\omega_i^2} - \frac{jkr^2}{2R_i}\right] \tag{A-5}$$

A-1. H. Kogelnik, T. Li, Proc. IEE, Vol. 54, No. 10, p. 1312 (Oct. 1966).

where the individual reflection coefficients, P_i, are given by

$$P_1 = R_1$$

$$P_2 = (1 - R_1)^2 R_2$$

$$P_n = (1 - R_1)^2 (R_2)^{n-1} (R_1)^{n-2}$$

The values of ω_i, ϕ_i and R_i are obtained from equations (A-2), (A-3), and (A-4) by substituting for the various axial distances, i.e.,

$$z_n = z_1 + 2(n-1)\delta$$

where δ is the displacement of the second mirror surface due to the film being deposited.

The expression for the radial intensity was obtained by minimal calculation of the first 10 terms of the series, and these values were numerically integrated over a given detector area to obtain the shape of the detector output as the mirror spacing was altered.

The computed waveform asymmetry becomes large as the mirror separation is increased, and the shape of the waveform asymmetry matches that obtained in practice.

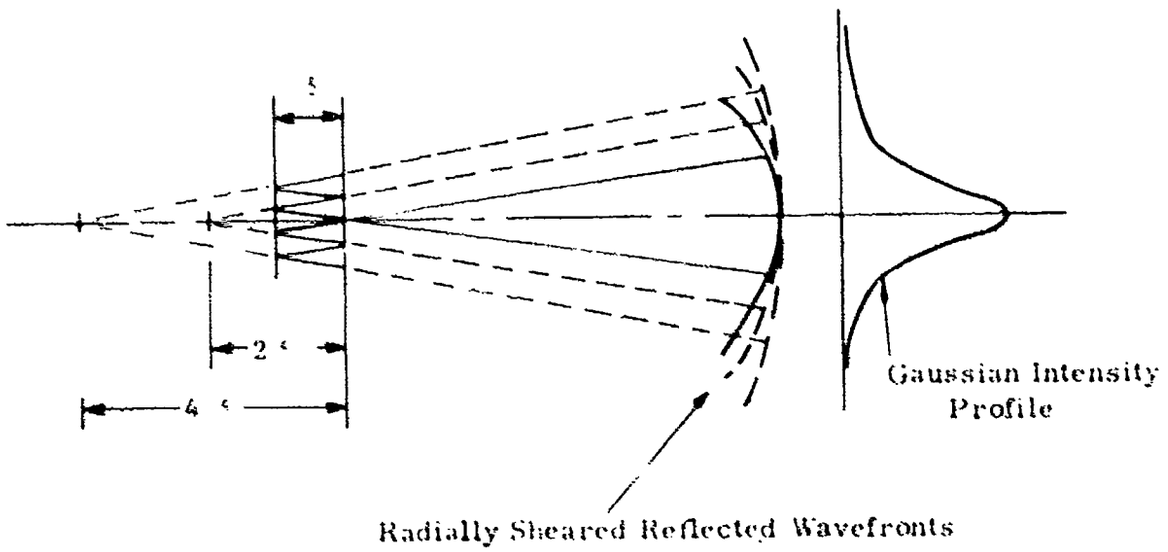

Figure A-1

UNCLASSIFIED

SECURITY CLASSIFICATION OF THIS PAGE (When Data Entered)

REPORT DOCUMENTATION PAGE		READ INSTRUCTIONS BEFORE COMPLETING FORM
1. REPORT NUMBER	2. GOVT ACCESSION NO.	3. RECIPIENT'S CATALOG NUMBER
4. TITLE (and Subtitle) INTRINSIC AND THERMAL STRESS MODELING FOR THIN-FILM MULTILAYERS		5. TYPE OF REPORT & PERIOD COVERED Final Technical Report May 1976 - May 1977 6. PERFORMING ORG. REPORT NUMBER 13396
7. AUTHOR(s) A.M. Ledger R.C. Bastien		8. CONTRACT OR GRANT NUMBER(s) DAAA-25-7[illegible]-C-0410
9. PERFORMING ORGANIZATION NAME AND ADDRESS The Perkin-Elmer Corporation Norwalk, Connecticut 06856		10. PROGRAM ELEMENT, PROJECT, TASK AREA & WORK UNIT NUMBERS ARPA Work Order No. 3220
11. CONTROLLING OFFICE NAME AND ADDRESS Defense Advanced Research Projects Agency 1400 Wilson Boulevard Arlington, Virginia 22209		12. REPORT DATE 15 June 1977 13. NUMBER OF PAGES 58
14. MONITORING AGENCY NAME & ADDRESS(if different from Controlling Office)		15. SECURITY CLASS. (of this report) UNCLASSIFIED 15a. DECLASSIFICATION/DOWNGRADING SCHEDULE

16. DISTRIBUTION STATEMENT (of this Report)

Distribution of this document is unlimited.

17. DISTRIBUTION STATEMENT (of the abstract entered in Block 20, if different from Report)

18. SUPPLEMENTARY NOTES

19. KEY WORDS (Continue on reverse side if necessary and identify by block number)

Antireflection coatings	Optical coatings
High-energy lasers	Optical materials
Infrared windows	Potassium chloride
Interferometers	Stresses
Material properties	

20. ABSTRACT (Continue on reverse side if necessary and identify by block number)

The measurement of intrinsic and thermally induced stresses in multilayer dielectric coatings was investigated to improve reliability and durability predictions of thin-film coatings, particularly, those coatings that will be utilized under extreme thermal conditions (e.g., in high-energy laser systems). Principally, the investigation was conducted using thorium tetrafluoride, zinc selenide, and thallium iodide films as antireflection coatings on

DD FORM 1 JAN 73 1473 EDITION OF 1 NOV 65 IS OBSOLETE

UNCLASSIFIED

SECURITY CLASSIFICATION OF THIS PAGE (When Data Entered)

20. ABSTRACT (Continued)

potassium chloride at 10.6 micrometers. A four-channel stress interferometer system that measures stress levels in single or multilayer films as they are being deposited was fabricated and tested. A new experimental technique was established whereby the stress interferometer system can also be used to compute Young's modulus and the coefficient of thermal expansion for the thin film materials. A computer code was developed that utilizes the experimentally measured values of intrinsic stress, expansion coefficient, and Young's modulus to model stress levels in multilayer coatings when subjected to a changing uniform environment.